HHS Public Access

Author manuscript

*J Neural Eng*. Author manuscript; available in PMC 2016 May 17.

Published in final edited form as:

*J Neural Eng*. 2013 December ; 10(6): 066014. doi:10.1088/1741-2560/10/6/066014.

# Failure mode analysis of silicon-based intracortical microelectrode arrays in non-human primates

**James C Barrese**[1,2,3,4], **Naveen Rao**[2], **Kaivon Paroo**[2], **Corey Triebwasser**[2], **Carlos Vargas-Irwin**[2], **Lachlan Franquemont**[2], and **John P Donoghue**[2,3]

[1]Department of Neurological Surgery, UMDNJ—New Jersey Medical School, Newark, NJ, USA

[2]Department of Neuroscience and Brown Institute for Brain Science, Brown University, Providence, RI, USA

[3]Department of Veterans Affairs, Center for Neurorestoration and Neurotechnology, Rehabilitation Research and Development Service, Providence, RI, USA

## Abstract

**Objective—**Brain–computer interfaces (BCIs) using chronically implanted intracortical microelectrode arrays (MEAs) have the potential to restore lost function to people with disabilities if they work reliably for years. Current sensors fail to provide reliably useful signals over extended periods of time for reasons that are not clear. This study reports a comprehensive retrospective analysis from a large set of implants of a single type of intracortical MEA in a single species, with a common set of measures in order to evaluate failure modes.

**Approach—**Since 1996, 78 silicon MEAs were implanted in 27 monkeys (*Macaca mulatta*). We used two approaches to find reasons for sensor failure. First, we classified the time course leading up to complete recording failure as acute (abrupt) or chronic (progressive). Second, we evaluated the quality of electrode recordings over time based on signal features and electrode impedance. Failure modes were divided into four categories: biological, material, mechanical, and unknown.

**Main results—**Recording duration ranged from 0 to 2104 days (5.75 years), with a mean of 387 days and a median of 182 days ($n = 78$). Sixty-two arrays failed completely with a mean time to failure of 332 days (median = 133 days) while nine array experiments were electively terminated for experimental reasons (mean = 486 days). Seven remained active at the close of this study (mean = 753 days). Most failures (56%) occurred within a year of implantation, with acute mechanical failures the most common class (48%), largely because of connector issues (83%). Among grossly observable biological failures (24%), a progressive meningeal reaction that separated the array from the parenchyma was most prevalent (14.5%). In the absence of acute interruptions, electrode recordings showed a slow progressive decline in spike amplitude, noise amplitude, and number of viable channels that predicts complete signal loss by about eight years. Impedance measurements showed systematic early increases, which did not appear to affect recording quality, followed by a slow decline over years. The combination of slowly falling

[4]Author to whom any correspondence should be addressed. jamesbarresemd@gmail.com.

Online supplementary data available from stacks.iop.org/JNE/10/000000/mmedia

impedance and signal quality in these arrays indicate that insulating material failure is the most significant factor.

**Significance—**This is the first long-term failure mode analysis of an emerging BCI technology in a large series of non-human primates. The classification system introduced here may be used to standardize how neuroprosthetic failure modes are evaluated. The results demonstrate the potential for these arrays to record for many years, but achieving reliable sensors will require replacing connectors with implantable wireless systems, controlling the meningeal reaction, and improving insulation materials. These results will focus future research in order to create clinical neuroprosthetic sensors, as well as valuable research tools, that are able to safely provide reliable neural signals for over a decade.

## 1. Introduction

Restoration of neurologic function after stroke, spinal cord injury, or neurodegenerative disease is a major goal of emerging neurotechnologies. Neuroprosthetic devices that sense neural activity, called brain–computer interfaces (BCI), have the potential to restore lost function by becoming a replacement communication channel from preserved brain areas, bypassing damaged motor pathways. These devices require a sensor that records neural activity, a computer that successfully interprets those signals, and a functional output such as a computer cursor or robotic arm. One important BCI design incorporates intracortical multichannel sensors because they provide high fidelity spiking as well as field potential signals, both of which are useful sources of motor commands (Bansal *et al* 2012) that are not available from non-penetrating arrays. In order to be clinically applied, this sensor must be a safe, reliable, and stable source of signals over long periods of time, ideally a decade or more.

A variety of positive and negative claims about longevity and causes of failure have been made, but differences in species, surgical methods, electrode design, materials, and geometry have made it difficult to compare results across studies and reach a meaningful consensus. Mechanical, biological, and material differences are major classes that may contribute to the failure of each design. Across all sensors being developed for human BCI use, there has been a longstanding concern that penetrating electrodes will fail because of the well-established series of biological responses generated by the insertion and continued presence of a foreign body in the brain (Polikov *et al* 2005, Collias and Manuelidis 1957, Schultz and Willey 1976). These studies conclude that cell death and a glial reaction that separates recording surfaces from target neurons are major sources of recording failure. While the intracortical tissue response has been an area of great concern, motion of the electrode in the brain, meningeal responses, and materials degradation in the harsh intracorporeal milieu are less investigated problems that can also limit the ability to obtain useful signals. Specifically, meningeal encapsulation can extract foreign bodies and insulating material degradation can lead to smaller signal amplitudes.

Our group has been developing one type of microelectrode array (MEA) sensor and using it for multichannel neurophysiological non-human primate (NHP) studies and human BCI studies for more than a decade. The array, fabricated from boron-doped silicon, was first

developed by Richard Normann at the University of Utah (Jones *et al* 1992) and advanced as a human suitable sensor in a collaborative effort (Maynard *et al* 1999). It was then manufactured by a commercial entity (Cyberkinetics Neurotechnology Systems, Inc., now ceased operations) and finally commercially produced by a successor, Blackrock Microsystems (BRMS). While the preclinically tested array has varied in coating materials and fabrication details over this interval, this MEA has had the same basic configuration of 100 tapered microelectrodes with exposed platinum-coated tips, organized in a regular 10 × 10 grid, emanating from a single platform. Each 1 or 1.5 mm long electrode is separated by glass insulation and attached wires lead to a percutaneous titanium connector. Silicone and plastics insulate conductive surfaces. The platform sits on the cortical surface after being pneumatically inserted through the pia-arachnoid membrane.

The longevity (i.e., the duration of time useful signals can be derived) of this array has been investigated in a limited number of studies, providing some evidence why recordings eventually fail. Initial studies in cats found that 60% of 12 arrays could record neural activity six months after implantation. Many of these cases were terminated for endpoint histology at various stages of the experiment rather than failure, but the authors noted that the presence of fibrous encapsulating tissue on the cortical surface (which could extract arrays from the brain) remained an impediment to long-term success (Rousche and Normann 1998). Suner *et al* (2005) studied signals in three monkeys over a 514, 154 and 83-day period, which were experimenter-set endpoints for data collection. The number and form of action potentials recorded varied from day to day in no apparent pattern, and there was no evidence for an overall average time-related decline in channel count over these intervals. By contrast, Chestek *et al* (2011) reported in a long-term study in rhesus macaques an average decline of 2.4% per month in peak-to-peak (PTP) amplitude of the largest action potential on each channel over the course of 9.4, 10.4, and 31.7 months in three animals. Why this slow degradation of signal amplitude occurred was not clear. In addition to a substantial body of fundamental research, a version of the MEA has been used with an Investigational Device Exemption in the BrainGate and ongoing BrainGate2 pilot human clinical trials, using the 510(k)-cleared NeuroPort version (Blackrock Microsystems Inc., Salt Lake City, UT, USA). We have reported initial results suggesting that spiking can be an effective source of command signals to operate computers or control robotic assistants (Hochberg *et al* 2006, 2012, Kim *et al* 2008). One participant with tetraplegia due to brainstem stroke demonstrated that this penetrating MEA could remain functionally useful for more than five years (Hochberg *et al* 2012). Each of these results provided encouragement that multi-year recordings could be achieved. Nevertheless, the broader experience in NHPs indicates that these arrays can fail at many different intervals for reasons not yet systematically examined.

Over the past 16 years, our laboratory has amassed a large collection of data concerning the recording successes and failures of this MEA in a single species that may be a useful model for humans. Here we carried out a retrospective evaluation using performance data from 78 intracortical MEAs chronically implanted in rhesus monkeys. We analyzed the mechanical, biological, and material failure modes to advance our understanding of how to achieve long-term, stable recordings for animal research and human clinical applications. We also highlight the design modifications made during the course of these studies to provide further insight into ways to improve the quality and quantity of recordings.

## 2. Background

### 2.1. Data set

Since February 1996, 78 silicon electrode arrays were implanted in 27 monkeys (*Macaca mulatta*: 18 male, 9 female). The size and scope of this data set, collected by a wide variety of investigators across this interval, poses a number of analytical challenges because the research goals of the implants did not include failure mode analysis or a planned path of continuous improvement. Thus, this retrospective study required searching through records with substantial differences in the degree and detail of information gathered by many individuals over many years, sometimes making it difficult to report the same data for each case. We examined recordings (wherever data was available), with the intention of comparing the number of channels with recordings, signal quality, and impedance changes over time as our main data. We evaluated a range of variables that might affect failure, including surgical approaches, medication use, peri-operative events, and long term clinical events related to the presence of the implant. We attempted to gather micro and gross anatomical specimens and in some cases histology was available. Other sources of data include detailed training logs, veterinary records, photographs, videos, anecdotes, and direct observations. Because this is a rare and unusual data set we attempted to include as much information as possible, even when these data could not necessarily be tied to performance quality.

### 2.2. Developmental process of arrays

All of the arrays included in this analysis were silicon based MEAs. This $4.2 \times 4.2$ $mm^2$ platform sensor consists of 100 tapered, platinum-tipped microelectrodes made of boron-doped silicon with a 400 μm inter-electrode spacing. Each electrode emerges from the planar base and tapers to a point over a 1 or 1.5 mm length (starting with ~90 μm base) with an approximately 50 μm long recording tip coated with 500 nm of vapor deposited platinum (figure 1).

The MEA evolved to optimize function, implantation procedures, manufacturability and outcome. This included changes in insulation materials, electrode lengths (to meet experimental goals), number and type of wires leading from array to connector, and type of connector used (on a path to compact, high-density connectors). These evolutionary changes enabled the monitoring of a progressively larger number of electrodes with higher quality signals. Relevant design changes of which we are aware are described below to include potential variables affecting array performance. Details of known changes are provided in figure 2.

### 2.3. Summary of design changes

The first electrode shaft insulation material in our series was polyimide, which was changed after three cases to silicon nitride. However, silicon nitride reportedly degrades in aqueous environments (Schmitt *et al* 1999), which was consistent with anecdotal observations of poor signal-to-noise ratio (SNR) from those recordings. Subsequently array insulation was changed to, and remains parylene. Parylene-C is an effective electrical insulator with well-established biocompatibility and biostability profiles (Yuen *et al* 1987), but is reported to

degrade over time in biological environments (Schmidt *et al* 1988). Wiring to the array changed from hand soldered to wire bonded, which achieves greater reproducibility of these connections.

The array is attached to a percutaneous connector via a bundle of plastic-insulated wires within a siliconecoated bundle. Changes in the wire material and number of wires occurred over time. Initially, wires had a diameter of 1.5-mil (38.1 μm), were made of a platinum/iridium alloy, and insulated with PTFE. Presently, the wires are 1.0 mil (25.4 μm) diameter, made of a gold/palladium alloy, and since February of 2010, insulated with polyester enamel, Terester (Elantas PDG, Inc., St. Louis, MO, USA). Most of these changes were driven by ease of manufacturability and a desire to make the bundle as flexible as possible as an aid in implantation and to mitigate tethering forces. The entire wire bundle is coated with a thin layer of silicone elastomer. The number of wires in the microwire bundle, and therefore the number of useable electrodes has increased (due to availability of connectors) from 10 in the earliest implant to 96 since 2002. Skull-mounted connectors are used to pass signals to external signal processors. The availability of compact connectors suitable for monkeys with high pin density and low insertion forces was a limiting factor for nearly a decade. Connector design evolved over the time period covered, beginning with a 12-pin Microtech (FR-12S-6; Microtech, Pittsburgh, PA, USA) connector (9 arrays), to a 50-pin Winchester connector (7 arrays), to a 40-pin 'Tulip' connector (9 arrays), and eventually to a zero insertion force, spring-loaded 96-pin connector in a titanium pedestal made by BRMS (figure 3) in the 53 implants since 2002.

To meet investigational goals, electrode lengths varied. Most electrodes were 1.0 mm in length ($n = 58$) and placed in the motor or premotor cortex, with others at 0.5 mm ($n = 4$), 0.6 mm ($n = 1$), or 1.5 mm ($n = 15$). See supplementary data table 1 (available from stacks.iop.org/JNE/10/000000/mmedia) for summary of implant locations and electrode lengths. Details of the current manufacturing process and materials are available from BRMS.

## 3. Methods

### 3.1. Surgery

All arrays reported in this study were implanted into Rhesus macaques (18 male, 9 female) as approved by Brown University's IACUC committee. The surgical procedure for array implantation has varied across the test interval, in terms of the type and experience of the surgeons, and craniotomy and closing methods, which may be relevant variables in recording success.

Early in our series, skin incisions were large semicircular flaps, with rectangular craniotomies typically greater than 6 $cm^2$. Since approximately 2002, smaller mid-line incisions are made and the craniotomy minimized (<5 $cm^2$) to expose only the most relevant cortical areas, and minimize risk of infection. All implants covered in this series were inserted using a custom pneumatic piston (insertion speed: 8–10 m $s^{-1}$), developed initially by the Normann Lab at the University of Utah (Rousche and Normann 1992), now manufactured by BRMS. The method of insertion was the same for all arrays, using a

micromanipulator held pneumatic inserter, orthogonal to the array, using approximately the same pressure (172 kPa). Excursion was set to match the length of the array (0.5–1.5 mm).

Closing techniques varied to avoid perceived problems with dural adhesions to the array. Early closure techniques involved placing Teflon between the array and the dura (Maynard *et al* 2000). Epidural GoreTex (Gore® Preclude® Dura Substitute, WL Gore and Associates, Flagstaff, AZ, USA) and then epidural silastic (Kwik-Sil, World Precision Instruments, Inc., Sarasota, FL, USA) were also used to help close the dura. In some cases, titanium mesh was used to cover the craniotomy rather than replacing the bone flap, and dental acrylic was applied in certain cases to secure the connector and not infrequently to close the cranial defect. GoreTex sheets and silastic were eliminated from all implants since 2005, as our series showed no reduction in the extent of dural adhesions with this approach. We believe that the presence of multiple foreign bodies leads to more infections. A general effort has been made to mimic human neurosurgical protocols and procedures, with a deliberate effort to reduce the inclusion of foreign materials. A primary dural closure with 4–0 Nurolon sutures (Ethicon, Inc., Somerville, NJ, USA) is typically obtained. Remaining dural defects are closed with a periosteal or fascial autograft. The bone flap is replaced and secured with a low profile titanium plating system (MatrixNeuro, Synthes, Inc., West Chester, PA, USA). Dental acrylic is now avoided unless necessary to replace or repair an existing acrylic cap or, more rarely, to stabilize loose hardware (36/78 implants, 46%, involved acrylic to varying degrees).

This methodological evolution is the product of laboratory experience guided by clinical neurosurgeons who have performed or supervised 35 of the 78 implants in our series since 1999, particularly in the last ~6 years. Analyzing all of the details of the surgical procedure and its impact on failures is beyond the scope of this paper and will be explored more fully in a future publication, but details of surgical procedures that might be related to recording failure are included in the results.

### 3.2. Neural recordings

**3.2.1. Neural data—**Much of the recording data from arrays implanted early in our series is only available in summary form. These records were kept as hand-written cell counts per channel at each recording session and data were often stored on media that can no longer be fully retrieved. This type of ‘early’ data accounts for 31 arrays with >600 recording sessions. Spike amplitude and SNR were not documented for these implants. There were 47 further implants with digital data for a total of 1073 recording sessions. Since these arrays had 96 wire-bonded electrodes (some had only 94 or 95 wired electrodes) we calculated that our database consists of approximately 103 008 unique data points. For all implants with digital recording data, the following methods apply.

**3.2.2. Signal-to-noise and amplitude calculations—**For each channel on each array on each day, all spike waveforms were aggregated to compute SNR and PTP amplitude for that channel. Signals were first filtered with a single-pole analogue anti-aliasing filter with a 7.5 kHz cut-off frequency. The signal was then filtered using a fourth order Butterworth digital high-pass filter to extract spiking waveforms. This signal was sampled at 30 kHz. A

neural spike was determined by this signal crossing a threshold typically set at −4.5 dB of the distribution of signal values, but this was not always the case (sometimes set manually). A spike waveform spans 1.6 ms or 48 samples. Ten of these samples were before the threshold crossing and 38 samples were after the threshold crossing. Any channel that had >150 threshold crossings over a recording session was considered active and was further analyzed.

SNR was calculated in two parts. The noise amplitude for a channel was determined by finding the maximum and minimum values of each of the first five samples of the 48-sample window for all threshold crossings (typically tens of thousands). Recall that the first five samples precede the threshold crossing and should be uncontaminated by the actual spike waveform, although occasional pretrigger inflections in the waveform may be included and could increase noise estimate. The noise amplitude is the max–min difference of the mean over five points for all threshold crossings. We calculated the signal amplitude (PTP) by taking the median (across threshold crossings) of all samples and then finding the difference between the maximum and minimum of the median waveforms. The median was chosen in order to prevent large amplitude noise signals from artificially inflating the PTP. The ratio of the signal amplitude to the noise amplitude was the SNR. See supplementary data (available from stacks.iop.org/JNE/10/000000/mmedia) for details.

**3.2.3. Viable channels—**Next we calculated the number of viable channels per array for each recording session. Viable channels were defined as individual electrodes (or 'channels') within an array that were capable of recording action potentials. We considered a channel viable if it had a PTP amplitude $\geqslant$40 μV, noise amplitude <150 μV, and SNR > 1.

**3.2.4. Impedance measurements—**All impedance values reported in this analysis were measured using a commercial impedance meter designed for microelectrodes that is integrated into the BRMS Cerebus recording system (Blackrock Microsystems Inc., Salt Lake City, UT, USA). The device applies a 1 kHz stimulus, ± 50 pA max, using the built-in capabilities of the CerePort hardware and Cerebus Central software.

### 3.3. Defining failure and failure modes classifications

Given that a strong motivation for an intracortical sensor is to record and transmit action potentials, we define failure simply as the absence of extractable action potentials for all electrodes (channels) on an array. By our operational definition, an array has failed when there are no channels that have recordable action potentials. Local field potential (LFP) data was not consistently collected across arrays and thus was not used as an alternate measure of failure in this analysis.

We established four discrete failure mode categories: biological, material, mechanical, and unknown. Biological failures are defined as those related to the foreign body response of the tissue to the sensor, whether intra- or extraparenchymal, or clinical issues arising from the implant (e.g. peri-operative bleed). Material failures are related to inherent design flaws or material degradation (e.g. leakage of insulating materials). Mechanical failures are related to physical factors that move the sensor from its desired location or damage the hardware enough to prevent recording (e.g. connector removal by monkey). Unknown failures result

from signal loss not directly attributable to one of these mechanisms. Figure 4 illustrates potential failure modes by category.

Failures were also categorized as either acute or chronic. Operationally, we defined *acute failure* as a rapid loss of signals within a time-period of seven days. *Chronic failure* is defined as a slow, progressive loss of neural signals over a period of >1 week to years. This division is meant to distinguish catastrophic from progressive events that relate to underlying failure modes. As will be shown, acute failures are more likely to result from physical trauma to the hardware or subject. Examples include wire bundle disconnection or traumatic removal of skull-based connectors, but could include a rapid infectious process (i.e. acute biological). Chronic failures may reflect progressive tissue reactions or leakage of electrode insulation material. A subset of arrays never failed according to these definitions, and they were either removed because research was completed or were functional at the time of this analysis. These are included in the analysis of recording data but are not included as failed electrodes.

Each array failure was categorized as acute or chronic, then as biological, material, mechanical, or unknown, and then assigned a time to failure in post-implant days. The number of viable channels recorded in the last session prior to failure or elective cessation of recording was also reported, however 25 of the arrays used early in our series had less than 96 wire-bonded electrodes. We addressed this by also reporting viable channel counts as the fraction of viable channels over the total number of wire-bonded electrodes. We counted the number of times each particular failure mode was observed and tabulated the time to failure. The number of viable channels (as a fraction of total wire-bonded electrodes and as a percentage) at the last recording session prior to complete failure was also noted. Arrays with insufficient records to calculate the exact number of viable channels were noted as N/A.

## 4. Results

Of the 78 arrays used in this analysis, 62 arrays (79%) completely failed by our operational definition, 9 (12%) array experiments were electively terminated while the arrays were functional, and 7 (9%) arrays remained active at the time this study was closed (7 January 2012). The mean recording duration for all 78 arrays was 387 days post-implant and the median was 182 days.

### 4.1. Non-failures

Nine experiments involving functional arrays were terminated. The mean duration of this group was 486 days (median = 310). Six arrays were fully explanted at the termination of an experiment for research unrelated to the failure mode analysis. All six of these arrays were functional at explant, but removed in order to conduct other experiments. These monkeys all continued in good health, were trained for different experiments, and were successfully re-implanted with additional arrays in different cortical areas. The other three arrays (of nine) ceased recording when the monkey was euthanized in order to obtain histology necessary for a specific research project.

Seven arrays remained active throughout the study period. The mean duration of these active arrays was 753 days (median = 748). See table 1 for summary of array duration statistics and table 2 for details.

### 4.2. Array time to failure

The 62 failed arrays were assigned a post-implant day on which failure occurred. In some cases it was not evident from the records exactly which day the failure became complete. In such cases, failure was assigned to the first recording session with no viable channels where subsequent attempts to record showed no improvement. There were three arrays that never recorded any neural signals, thus the minimum time to failure observed was 0 days. These failures occurred at scattered times during this series (1997, 2002, 2009) and do not indicate a systematic shortcoming of manufacturing or design. The maximum time to failure was 2104 days (5.75 years). The mean time to failure of all 62 failed implants was 332 days (median = 133). The number of active arrays was plotted against days post-implant in figure 5. Most arrays failed within the first year, after which the rate of failure declined; as described below most of these were acute failures. The failure rate appears as an exponential decay process with a half-life ($t_{1/2}$) of approximately 250 days. Note that the rate of failures is significantly different from the rate of signal decay presented later in this paper.

### 4.3. Failure modes

The number of failures for each failure mode and the time to failure are presented in detail in table 2 and summarized in figure 6. Acute mechanical failures were the most common failure mode and the mean time to failure for this group was 288 days. The longest lasting arrays were in the chronic unknown category with a mean time to failure of 1311 days. The following sections describe the specific nature of each failure observed. For all narratives the number of monkeys will be noted as '*m*'.

### 4.4. Acute failures

Of all 62 failures, 45 (73%) were acute. Within the acute failures, 6 were biological, 6 were material, 30 were mechanical, and 3 were from unknown causes. The mean time to failure for all acute failures was 218 days (median = 63).

**4.4.1. Acute biological failures—**There were six acute biological failures (9.7%) with a mean time to failure of 36 days (median = 30). Two failures resulted from the death of an animal and four were due to euthanization secondary to infection. The details of these failures are presented below.

**Euthanasia/clinical (m = 1)—two arrays:** Two of the acute biological array failures resulted from the death of a single animal subsequent to an intraparenchymal hematoma and fatal cerebral edema three days post-operatively. Specifically, during the implantation procedure a piece of gauze caught by the drill impacted the surface of the brain. This led to a postoperative hemorrhage, and ultimately to euthanization of the animal. This is the only death in our series that was directly linked to the surgical implantation of an array.

**Euthanasia/infection (m = 2)—four arrays:** Four acute biological failures were from euthanization for clinical reasons related to intracranial infections, in two monkeys, each with two arrays. One monkey was perfused at 30 days post-implant with approximately 5/36 (14%) viable channels on each array. The other monkey was euthanized at 74 days post-implant with approximately 8/22 (36%) viable channels on each array. Experiments were terminated because both of these monkeys developed subdural empyemas. This purulent subdural infection manifested as altered mental status, irritability, photophobia, nausea, vomiting, and fever. Oral antibiotic therapy was attempted, but proved to be insufficient. Subdural infection was confirmed at autopsy. In one monkey, an infection was noted to have tracked along a screw used to secure the connector. The screw had pierced the dura and was likely the route by which the infection spread intracranially. The cause of the other infection is most likely related to an inadequate dural closure with an associated chronic subdural hematoma (also found on autopsy). The presence of old blood (which acts as a culture medium) and a potential route of infection (dural defect) may explain how this empyema developed. These failures were classified as acute biological due to euthanasia (as opposed to infection) because the infection did not directly terminate recordings or infiltrate the recording site.

**4.4.2. Acute material failures—**There were six (9.7%) acute material failures in our series with a mean time to failure of 113 days (median = 67). Two arrays were defective, three shorted, and one was damaged as the result of a design flaw.

**Defective (m = 2)—two arrays:** Two of these failures, early in the research, are assumed to be the result of production defects because they never recorded at all. Thus, time to failure was 0 days. One array was wired to two separate Microtech connectors, and we suspect a manufacturing defect, as this was a prototype. The other array was wired to one of the first CerePort connectors. The exact defect is not known, although we suspect that this connector was damaged while being autoclaved because of discoloration noted on the connector pins after sterilization. There were no noted surgical complications in either monkey. All arrays are now sterilized using ethylene oxide (EtO).

**Shorting (m = 3)—three arrays:** Three acute material failures were from ‘shorting’ of the connector, as revealed by impedances <50 kΩ on all channels (which is indicative of a path to ground). All of these arrays had the Tulip style connector (see figure 3(c)), which was fabricated from a computer edge-connector card that seemed to be prone to poor or shorted connections. Two cases followed an event in which the gold edge connectors were exposed to saline washes during revision surgeries for head-posts. One event occurred at day 205 with 2/36 (6%) channels recording prior to failure and the other occurred at day 341 with 18/74 (24%) viable channels. The third case appeared after a technician cleaned the connector pads at day 50. This array had 5/36 (14%) viable channels prior to shorting. The solution used to clean the pads was not recorded. All three of these arrays had extremely low impedance measurements (<100 kΩ, mostly 50–60 kΩ) that indicate all channels were shunted to ground. ChemSwab (ITW Chemotronics, Kennesaw, GA, USA) urethane foam swabs soaked in isopropanol and deionized water are now used to clean connector pads.

**Design flaw (m = 1)—one array:** The final acute material failure was also due to the Tulip style connector. A design flaw in the Tulip connectors made them prone to turning within the titanium pedestal thus severing the wire bundle at 84 days in this case. There were 8/74 (11%) viable channels functioning prior to failure. Tulip connectors were replaced with the CerePort in 2002.

**4.4.3. Acute mechanical failures—**The most common failure mode was acute mechanical, accounting for 30 arrays (48.4%), with a mean time to failure of 288 days (median = 130). This large group was broken down into two main subgroups: surgical and traumatic. The surgical group includes failures from elective surgical array internalization (cutting wire bundle, leaving array *in situ*, three arrays) and surgical removal of the array (seven arrays). The traumatic group includes failures from connector pin damage (3 arrays), damaged or disconnected wire bundles (14 arrays), and arrays that were mechanically extricated (3 arrays).

**Surgical: array internalization (m = 2)—three arrays:** Surgical wire bundle disconnection, connector removal, and internalization of the array (closing the field with the array left in place after cutting the wire bundle) were performed deliberately by the investigators in order to prevent the intraparenchymal spread of extradural infections for three arrays. One monkey with two arrays developed an epidural abscess that required surgical drainage at 62 days post-implant. The infection was related to pockets of serous fluid that developed within an unevenly placed acrylic cap used to secure the connectors. These fluid collections seeded an infection that extended below the acrylic and epidural silastic, but did not invade the subdural space. Consequently, the wire bundles of both arrays were cut as they exited the dura in order to avoid introducing infection to the subdural space. The wound was thoroughly washed out and affected tissue was debrided. The monkey was treated with antibiotics and recovered in good health. Another array in a different monkey was internalized to prevent the spread of a chronic sub-acrylic wound infection that led to an epidural abscess at 1832 days post-implant with 26/96 (27%) viable channels. These events point out the challenges of maintaining closure with acrylic caps that can lead to chronic wound infections at the acrylic margins. Acrylic is avoided in current implantations.

**Surgical: surgical removal (m = 6)—seven arrays:** Complete surgical removal of an array was performed seven times. Four arrays ($m = 3$) were explanted when hydroxyapatite paste placed during implantation to facilitate bone growth began to crumble. A thick layer of hydroxyapatite placed during surgery prevented full osteointegration. This led to abnormal bone growth patterns that destabilized the connectors and worsened when the hydroxyapatite ultimately crumbled. Hydroxyapatite placed in thin layers was used successfully in other cases to fill in craniotomy defects. The four failures ($m = 3$) occurred at days 63, 63, 119, and 176 with 60/96 (63%), 46/96 (48%), 62/96 (65%), and 20/96 (21%) viable channels, respectively.

Three arrays ($m = 3$) were fully explanted because the connectors became loose and attempts to re-secure them failed. Two of these connectors were CerePort types that sustained repeated trauma when the monkeys hit the connector against cage parts during typical cage activity (according to caretaker logs). This recurrent impact eroded the bone

holding the pedestal screws in place. These arrays were explanted at 38 days with 64/96 (67%) viable channels and 735 days with 20/96 (21%) viable channels. The third array in this group was explanted because the connector became loose after an altercation between two monkeys. Attempts to reinforce the pedestal with larger diameter screws and titanium straps proved insufficient. This array was removed at 420 days with 20/96 (21%) viable channels.

**Traumatic: connector pin damage (m = 3)—three arrays:** Three arrays failed when irreparable damage to the connector pins occurred. One early study monkey developed generalized tonic-clonic seizures >1 year after implantation. The monkey hit its Microtech connector against the bars of its cage during a seizure at 565 days post-implant with 5/11 (45%) viable channels. Seizures became more frequent over the following year and it was found to be Simian Retrovirus (SRV) positive, but no definite etiology underlying the seizure disorder was identified. It is unlikely that the seizures were related to the presence of the implant given that the seizures were nonfocal. Another array failed at 420 days post-implant with 25/96 (26%) viable channels when a technician damaged the contact pads of a CerePort while cleaning them with an abrasive material (material not recorded). The final array in this category failed at 24 days when the surface contact pads of the CerePort connector were indented, preventing attachment of the recording cable that leads to the amplifier system. Training logs indicate that this monkey hit its head on the bars of the cage after removing the protective cap. The cap has undergone numerous design changes to make it more difficult for monkeys to remove them.

**Traumatic: wire bundle damage/disconnection (m = 12)— 14 arrays:** The majority of acute mechanical failures were related to the monkey manipulating the skull-mounted connector in some way. Eight failures ($m = 8$) resulted when the connector detached, either by self-manipulation by the monkey or by wedging the connector between the bars of the cage. When these connectors detached, the wire bundle snapped, leaving the array intracranial. This type of sporadic failure occurred from 19 to 819 days post-implant. See table 2 for details.

One failure resulted after an altercation between monkeys that led to connector dislocation and breakage of the wire bundle. This failure occurred at day 201 with 86/96 (90%) viable channels. One monkey manipulated the area of the incision enough to expose and sever the wire bundle by hand at day 376 with 39/96 (41%) viable channels prior to failure. Three wire bundles ($m = 1$) were damaged iatrogenically, 48 days post-implant during a wound revision surgery. Array wires were unintentionally stripped after being wrapped around titanium screws placed in the skull to secure the acrylic cap. Prior to failure, these arrays had 3/49 (6%), 10/24 (42%), and 11/24 (46%) viable channels. Another failure occurred from the wire bundle snapping when half of the acrylic cap came off with the connector at 496 days with 12/47 (26%) viable channels. This cap had been placed in two separate procedures and a gap was found between the two pieces of acrylic.

**Traumatic: array pulled from brain (m = 3)—three arrays:** Three arrays were unintentionally explanted. In one case a monkey manually pulled on a segment of exposed wire bundle, explanting the array at 187 days with 76/96 (79%) viable channels. In this case,

the silastic used to coat the wire bundle during surgery led to skin irritation and subsequent manipulation by the monkey, causing skin erosion that exposed the wire bundle. Silastic is no longer used in our surgeries. One array was inserted into edematous brain with no dural closure or dural substitute. A burr-hole cover was placed over the site and acrylic was applied; however it seeped down and bonded to the back of the array. Time to failure was three days post-implant when swelling diminished and extracted the array from the cortex. A surgeon accidentally pulled out the final array in this category during a revision surgery for placement of an acrylic cap at 167 days post-implant with 24/94 (26%) viable channels.

#### 4.4.4. Acute unknown failures

**Acute unknown (m = 3)—three arrays:** There were three (4.8%) acute failures for which the exact failure mode is not known. The mean time to failure for this group was 84 days and the median was 54 days. The first failure occurred suddenly at 54 days post-implant but insufficient records remain to determine the cause. Another acute unknown failure occurred at day 0. This implant was placed unevenly into the cortex near the supplementary motor area and partially over a small artery. Intraoperative photos reveal that some of the electrodes were not actually inserted. Although impedance measurements were in the acceptable range no cells were ever recorded, consistent with a failed insertion. A material failure is unlikely as the proximate failure mode. The third array failed at day 198 with 5/23 (22%) viable channels. There are few remaining records for this array, but it appears that there were several wound infections and washout procedures that may be related to failure.

### 4.5. Chronic failures

Of all 62 failures to date, 17 (27.4%) were classified as chronic, meaning they showed a slow progressive loss in recording capability over weeks or longer that resulted in complete failure. Within chronic failures, nine were biological, two were material, 0 were mechanical, and six were from unknown causes. The mean time to failure for all chronic failures was 633 days (median = 261).

**4.5.1. Chronic biological failures—**There were nine (14.5%) chronic biological failures with a mean time to failure of 160 days (median = 163). We attribute all of these failures to meningeal encapsulation of the array and extrusion from the cortex.

**Meningeal encapsulation of short electrodes (m = 4)—five arrays:** Five of these failures were in arrays with custom short electrodes and all were placed in the postcentral gyrus. Four of these arrays had 0.5 mm electrodes and one had 0.6 mm electrodes. This accounts for all of our implants with electrodes <1.0 mm. One of the 0.5 mm electrode arrays was partially inserted across a sulcus and had an exceptionally rapid meningeal encapsulation, failing by day 21. The number of viable channels quickly dropped to 5/96 (5%) just prior to failure. Of note, this array still had over 30 channels with LFP data at the time of explant, which makes a materials failure unlikely. Two 0.5 mm electrode arrays progressively failed by 163 and 188 days, with 2/96 (2%) and 9/96 (9%) viable channels, respectively, at the session prior to failure. The remaining two arrays (0.5 mm and 0.6 mm electrodes) in this group ($m = 1$) both failed by 255 days. Complete encapsulation and extrusion from the cortex were confirmed visually during explantation (figure 7).

**Meningeal encapsulation (m = 4)—four arrays:** The other four chronic biological failures are also from meningeal encapsulation but occurred in 1.0 mm electrode arrays. Surgical photos show that three of these arrays were placed directly over sulci or were subsequent implants through preexisting meningeal encapsulation material. At explantation of these arrays, complete encapsulation was noted and no electrodes were within the cortex. Surgical photos from the explantation of four similarly encapsulated arrays are shown in figure 8. The arrays in this category failed by 76, 99, and 125 days post-implant. Respectively, these arrays had 5/96 (5%), 6/96 (6%), and 32/96 (33%) viable channels prior to failure. The last encapsulated array had 1.0 mm electrodes and failed by day 261. There were 37/95 (39%) viable channels at the last documented recording session several months prior to complete failure. This monkey developed meningitis that prevented regular recordings until his health improved. A prolonged course of antibiotics effectively treated the infection. At explantation, a thick meningeal capsule was found to have lifted the array out of the brain. These results suggest that meningitis might amplify the rate and extent of meningeal encapsulation.

### 4.5.2. Chronic material failures

**Chronic connector shorting (m = 2)—two arrays:** There were two (3.2%) chronic material failures with a mean time to failure of 724 days (median = 724). One failure after 893 days resulted from a progressive signal loss by apparent ‘shorting’ of the connector pads in a Tulip style connector. This monkey had multiple head-post revision surgeries where small amounts of fluid contacted the connector pads. This is a similar mechanism to the acute failures described above but is classified as chronic because it was incremental and progressive over several years. The median impedance went from 124 kΩ to 70 kΩ in a spatial pattern consistent with the orientation of the connector pads and a temporal pattern consistent with the surgeries. There were approximately 20/74 (27%) viable channels at the session immediately prior to the final ‘shorting’ event.

The other chronic material failure occurred by day 555 from ‘shorting’ in a CerePort style connector. Small amounts of blood and serous fluid were repeatedly found directly on the connector pads underneath the protective connector cap. This was a chronic intermittent problem in which several channels ‘shorted’ at a time. Median impedances in this case showed a similar pattern, incrementally dropping from ~170 kΩ to ~61 kΩ after each time fluid was found on the connector. There were 8/96 (8%) channels active at the last session before failure. A custom ‘O-ring’ between the CerePort connector and its protective cap now prevents this from occurring.

**4.5.3. Chronic mechanical failures—**There were no observed failures that met criteria for both chronic and mechanical in nature.

### 4.5.4. Chronic unknown failures

**Progressive signal attenuation (m = 3)—six arrays:** There were six (9.7%) chronic unknown failures with a mean time to failure of 1311 days (3.6 years) and a median of 1146 days. All showed a slow progressive loss of signals that eventually resulted in complete failure, however the causes are unknown. The number of viable channels dropped slowly

over time and the spike amplitudes fell steadily until they were no longer separable from background noise. Similar patterns of signal loss were actually observed in all arrays over sufficient time periods, regardless of the ultimate failure mode. Two arrays ($m = 1$) early in our series were polyimide-insulated with Microtech connectors and failed by 690 days and 1091 days. The third array in this group was insulated with parylene and had a CerePort connector. It failed by 1200 days with 23/96 (24%) viable channels at the last documented recording session. Of note, spike amplitudes were very low (~40–50 μV) at this session.

The other three arrays in this group were all parylene coated with CerePort connectors ($m = 1$). The first failure took place by 1008 days with 7/96 (7%) viable channels. This array was explanted and two new arrays were placed at the same surgery. These two arrays failed by 1775 and 2104 days post-implant. There were 3/96 (3%), and 11/95 (12%) viable channels at the last recording session prior to failure, respectively. The six arrays in the chronic unknown category ultimately failed as a consequence of this progressive decay and therefore best demonstrate the current potential of this technology. A comprehensive analysis of temporal and spatial recording trends in our arrays is under way and will be published in a future report. Below we present a brief summary of the long-term recording trends that best demonstrate the decay in signal quality over time.

### 4.6. Impedance and neural recordings

Recording quality, in terms of the impedance, number of channels detecting signals, and the amplitude of those signals are the benchmarks for implant quality, as well as the viability of the nearby tissue. In order to control as best as possible for the large number of variables in our dataset, we restricted this signal quality analysis to nearly identical CerePort implant systems made in recent years. Thus, we included arrays with 1.0 mm electrodes, parylene-c insulation, 1.0-mil diameter Au/Pd wire bundles, and identical connectors. Forty-seven arrays fit the above criteria, were directly comparable to each other in terms of materials, and reflect the most current design features. Data for all 47 of these arrays were aligned to the day of implant and recording sessions were binned in 14-day clusters. The number of arrays included in each bin was variable and decreased over time as failures occurred. The impedance, mean viable channel count, spike amplitude, noise amplitude, and SNR for viable channels were trended over time.

**4.6.1. Impedance trends—**Impedance data exists for 26 of the 47 arrays across 305 sessions for all 96 channels yielding a total of 29 280 impedance data points. The pre-implant mean impedance across all arrays and all electrodes was 305 kΩ. Mean impedance more than doubled (2.48 ×) during the first two weeks after implantation (mean 755 kΩ), stabilized for approximately 150 days, then declined slowly over time with a slope of −0.23 (figure 9). Figure 10(a) illustrates this trend in three arrays selected for having the most abundant short-and long-term impedance data. Detailed impedance data from a subgroup of seven arrays with the most frequent early measurements confirm that the same global trends are also seen within individual arrays (figure 10(b)).

**4.6.2. Amplitude trends—**There were 47 arrays with digital spike data and a total of 1073 recording sessions. Since these arrays had 96 connected electrodes, our database

consists of approximately 103 008 unique data points. The number of standard spike recording sessions and the number of arrays used in each 14-day bin are shown in supplementary data figure 1 (available from stacks.iop.org/JNE/10/000000/mmedia). The mean number of viable channels declined steadily over time for all arrays as seen in figure 11. There are several notable step-offs in this trend that reflect the loss of some well functioning arrays because of acute failures.

Across all arrays, the mean spike amplitude (PTP) for viable channels started at approximately 69 μV in the first week and rose to approximately 104 μV over the first month. The PTP amplitude clearly trended downward over time, and reached a mean of 48 μV by the final recording session at day 2098 (figure 12(a)). This trend was consistent across all arrays and the average slope of this decline is −0.017. The mean noise amplitude of viable channels also rose over the first month, from 38 to 58 μV. A similar rate of decline, −0.012, was seen with the noise amplitude (figure 12(b)). By 2098 days, the mean noise amplitude fell to 27 μV. By contrast, the SNR for viable channels actually went up over time from 1.6 in the first week to 1.9 by 2098 days. This was likely due to a selection bias for the remaining viable channels that have very stable signals and the near parallel trend in spike and noise amplitude over time (figure 12(c)).

**4.6.3. Relationship between impedance and amplitude—**It is commonly held that impedance predicts the overall ability of an electrode to record neural signals, but many other features such as proximity to cells, cell size and geometry, tip geometry, and tissue reactions may affect recording. Our data show that the relationship between signal quality and impedance is weak. Figure 13 plots the linear regression line for both parameters and projects when critical values will be reached. Mean impedance values reflecting that the array is shunted to ground (50 kΩ) by extrapolation would be reached at 2783 days. Amplitudes of 40 μV or below are typically within the noise range and spikes are not readily discernable. This critical value would not be reached until 3000 days, assuming a linear decline.

Additionally, for all 104 recording sessions where both spike data and impedance measurements were recorded in the same session, we plotted the PTP amplitude from each electrode against the impedance of that electrode. This yielded 9919 data points across all arrays after filtering out data points with impedances over 2500 kΩ ($n = 31$). This was performed for the first 0–10 days, 10–100 days, for all sessions 365 days or later, and finally for all recording sessions (figure 14). The overall correlation coefficient ($r = 0.0754$, $p < 0.05$, $n = 9919$) suggests a very weak positive correlation, suggesting that impedance for an operational electrode is not a useful predictor of its spike recording ability. Interestingly, the correlation coefficient changed over time from weakly positive ($r = 0.224$, $p < 0.05$, $n = 619$) in the first 10 days, to extremely weak over the next 100 days ($r = 0.0421$, $p < 0.05$, $n = 4765$), to very weakly negative after the first year ($r = -0.0902$, $p < 0.05$, $n = 1313$). This finding suggests that multiple factors independent of impedance determine the signal quality.

Generally, there is a slow, progressive decay in signal quality and impedance that can be observed in those arrays that continue to record for long time periods. Despite this global trend, there are many channels that record spikes successfully for years. Some channels

record sporadically, with units coming and going every several months, which can in part be attributed to the failure of spring loaded pins in the mating connector to land firmly on the contact pad for the CerePort system. Figure 15 provides a few examples of the spike waveform variability in recordings over time to demonstrate that shapes may go up or down over time.

## 5. Discussion

The present study provides a unique and extensive evaluation of chronically implanted MEA performance in NHPs in the context of a systematic classification plan. This retrospective analysis summarizes experiences from the largest set of implants ever evaluated for a single type of penetrating multiple MEA in a single species. The study examines an array currently used for both NHP basic research as well as in pilot human clinical studies and research applications. We devised a failure mode classification system to capture three categories intended to cover the full range of sensor issues: biological, material, and mechanical factors. We also separated these categories according to acute (rapid) or chronic (evolving over time) signal loss, which could have different underlying failure modes. We intend for this system to serve as a standard to compare the performance of other sensors. Our approach expands the investigation of failure modes to include array materials, tissue encapsulation, connector design changes, breakage, impedance, signal properties, and surgical effects not addressed in many previous studies. In addition to the large sample size, the study includes a large set of long-term observations of arrays studied 2–6 years, showing that long-term spike recording is feasible with this technology in NHPs but not always reliably achieved. The analysis describes measures of recording quality, which is the most relevant detail for neurophysiological applications, but also includes observations that point to technical improvements needed to achieve safe and more reliable recordings. Well-established tissue responses and the influence of surgical procedures are important factors not directly evaluated here, but will be addressed in future reports from our NHP and human data. However, the combination of direct gross tissue observation coupled with electrical measurements of signal quality and impedance provide strong evidence for major factors that prevent long-term recording. Overall our results point to acute connector failure, meningeal encapsulation, and materials degradation as the most concerning barriers to successful multiyear recording.

### 5.1. Failure mode classification system

In the context of this study, failure was defined as a loss of discernible action potentials on all channels of an array, either abruptly (acute) or progressively (chronic). Other definitions of failure could include reaching some threshold number of channels, but this seemed more arbitrary than our criterion. The most relevant measures might also be shaped by the demands on the signal in its desired application, such as having large amplitude spikes. We created acute and chronic categories to separate catastrophic mechanisms from those that evolve over time, which may have different underlying causes and different signatures in the features we measured. In addition to spike recording, intracortical sensors can record LFPs, which have both basic science and potential clinical utility and may have different loss

profiles than spiking signals. It will be important to evaluate these signals in future analysis of these data.

Based on clinical observations we classified failures as biological, material, and mechanical, plus unknown. The rationale for this division was to separate different root causes of poor recording quality, although these can be inter-related, making subdivision difficult. *Biological* classes included grossly observable tissue reaction and clinical issues (e.g., infection), *material* failures included connector or wire bundle defects and shorting, and *mechanical* issues included damage related to the connector, but also included factors such as breakage of wires or required removal of the array, each of which would eliminate an electrode's conductive path from sensor recording site to signal processors. These types of observations missed important biological phenomena like cell death and bleeding due to electrode insertion and gliosis around the implant, material issues like array insulation degradation, which are only observable at a microscopic level, and mechanical factors like micro-motion from electrode tethering. We measured five variables: impedance, number of viable channels, spike amplitude, noise, and SNR that are used below to infer the effects of intraparenchymal changes, array material issues, and tethering effects.

### 5.2. Why do arrays fail acutely?

Our data show that connector breakage, peri-operative events, and infection comprised a major class of issues that led to a rapid failure in recording. Acute factors accounted for almost three quarters of failures (45/62 arrays, 73%). The vast majority of these acute failures were acute mechanical failures (30/45 arrays, 67%). More than half of the failures in our series (56%) were in some way related to the skull-based connector. In addition to direct damage, loosened connectors also created an acute failure because they required removal in order to prevent array extraction and cortical injury. Experiments in which we used bone replacement or supplement materials (e.g. dental acrylic) led to acute failure of this type for eight arrays in seven monkeys (section 4.4.3). These materials are now avoided and caps to protect the external portion of connectors are now routinely used. Early connectors, poorly suited for this application (figure 3), were very prone to failure, making it difficult to evaluate other possible contributions to altered recording quality. Recognition of this problem led to the current compact, high-density connector. This lower profile, titanium encased connector is much more reliable, but remains problematic because its protrusion from the skin makes it susceptible to damage in freely moving monkeys.

Acute biological failures included infection and death. A post-operative hemorrhage led to the death of one animal and failure of its two arrays; this was the only failure of this type. Intracranial infection was rare across the entire group (4 of 27 monkeys, 7 of 78 implants). Two monkeys (four arrays) developed subdural empyemas and two monkeys (three arrays) had epidural abscesses. These infections led to recording failures because experiments had to be terminated. As described in the results, these could be attributed to surgical techniques or foreign bodies, each of which has been remedied by elimination of foreign bodies like dental acrylic, hydroxyapatite, or artificial dura, as well as improved surgical technique following human procedures and standards. The introduction of fully implantable systems

(Borton *et al* 2013), which will require internal signal processing and wireless transmission, will greatly ameliorate both mechanical and infectious concerns.

### 5.3. Why do arrays fail over time?

Our data show that it is feasible to record spiking signals from these sensors for years, but that recording quality, both number of channels and signal amplitude, consistently diminish over long times. If all acute failures are eliminated, chronic recordings were obtained for more than one year in nearly half (48%) of the implants. Chronic recordings were obtained >1 year in 33% of all 78 implants. Of these 26 arrays that recorded for longer than one year, 61% recorded for a full second year, 27% recorded for a full third year, 15% recorded for over four years, and 8% recorded for over five years, matching what has been reported for one human using a similar MEA (Hochberg *et al* 2012). When all 78 arrays are examined over the first year, 56% ceased recording due to failure, but 10% never failed (6% elective experiment end; 4% remained functional at the study end). The two major chronic failure modes were chronic biological from grossly observed meningeal encapsulation that extracted the electrode array (53% of chronic failures) and chronic unknown, where a progressive decay in signal quality was observed without a clear etiology (35% of chronic failures). Amongst the chronic failures, recordings lasted from 555–2104 days for the entire group that did not fail from meningeal encapsulation.

The pattern of electrical measurements examined over the short and long term revealed patterns of change that provide evidence for certain failure modes and help to reject others. We had two measures of electrode quality to infer failure sources: impedance and signal recording. Over the short term, we found that impedances rise in the first two weeks following implantation and remain high for as long as 100 days. Subsequently they show an ongoing and progressive decrease over years when considered across the data set. The number of channels with signals (~60) and signal amplitude was initially high for the first months, and then also progressively declined over years. Similarly, noise on the electrodes showed a decline over time, leading to a flat SNR when all data is averaged. As we will elaborate, this collection of changes points to materials failure, and not parenchymal responses, as a major source of signal loss.

It is widely documented in many species and with many types of MEAs that surgical insertion and the chronic foreign body presence leads to a series of events that generally have been used to support the conclusion that tissue responses are a major cause of recording failure for implanted devices. Established tissue responses to electrodes include gliosis (Griffith and Humphrey 2006, Edell *et al* 1992, Turner *et al* 1999), cell death (Biran *et al* 2005, Zhong and Bellamkonda 2007), and metabolic and vascular changes that are initiated by electrode penetration (Bjornsson *et al* 2006). Other concerns include the chronic inflammatory reaction mediated by microglia and macrophages (McConnell *et al* 2009) and ongoing phagocytosis (Polikov *et al* 2005). Reportedly, a gliotic sheath is fully formed in rodents by 6–12 weeks (Liu *et al* 1999, Turner *et al* 1999, Szarowski *et al* 2003). Consistent with this tissue response there is a rapid rise in impedance over the first 1–3 weeks, that has been related to the initial inflammatory response (Prasad and Sanchez 2012, Williams *et al* 2007), or the increased density of astrocytes, fibroblasts, and microglia surrounding the

implant (Mercanzini *et al* 2009, Merrill and Tresco 2004). Our observed early impedance rise extends this observation to NHPs and to this MEA geometry. Our results are consistent with the reported increased cell concentration and gliosis surrounding implants during the initial inflammatory response. However, recording quality when examined across our data set is best at this time interval, indicating that this early impedance increase is not predictive of recording quality in the months after implantation.

With regard to signal recording, the tissue response profile predicts an initial period in the first few months of declining signal amplitudes as the glial sheath thickens and moves neurons farther away from the electrode recording surface, as well as a decrease in the number of channels recorded as cells die. However, this prediction is not consistent with our findings. Cell recordings increased in the initial months and lasted for years (when acute factors are discounted), with a steady average decline over that longer interval (figures 12 and 15). Notably, signals were of high quality throughout the interval of increasing and then decreasing impedances (figure 14) and signal amplitude loss occurred much later (figure 12) than the well-documented time course for gliosis. Similarly, cell death due to the initial insult would predict an initial loss of signal and then a stable number of cells (all other features being equal) as the initial tissue insult resolved. This pattern, too, does not support that the tissue response is the cause of the chronic recording decline we observed.

Our data predict that the currently tested arrays could produce useful signals up to 7–8 years (figure 13), if acute mechanical and meningeal responses are controlled. Examined over the course of one year and longer, our data revealed an ongoing decline in impedance, the number of viable channels, and signal amplitude, as well as a roughly flat SNR. The subsequent decline in impedance we observed over the long term is not expected if the tissue response is stabilized in the first three months as widely reported (Liu *et al* 1999, Turner *et al* 1999, Szarowski *et al* 2003). Instead, it should have remained the same or potentially increased if glial responses slowly continue. Instead, impedance declined. We also observed a decrease in noise and a roughly flat SNR over time. This too does not fit with the hypothesis that gliosis is reducing recording quality over time. A stable tissue interface established after many months in-situ would predict a stable SNR, but not a decrease in noise and an ongoing decline in signal. Saxena *et al* reported a short-term drop in SNR with Michigan arrays, but it is hard to compare their small sample ($n = 8$) in a different species with very different technology (Saxena *et al* 2013). This too is not consistent with the initial tissue reaction as the underlying cause of long-term recording failure.

Instead, our signals and impedance change patterns leads to the conclusion that materials degradation is the major underlying cause of long term signal quality decline. Because sensors are recording very small amplitude electrical signals (μV), a parallel electrical path shunting signals away from high input impedance amplifiers will diminish signal amplitude (both spike and noise amplitude). Loss of electrode coatings or insulation, breaks at wire bonds, and leakage or cracking of sealing materials can produce this shunting path (Schmidt *et al* 1988) and could introduce crosstalk between channels, especially on the platform base of the array where connections are closely spaced. Shunting is a concern for this array because wiring on the back of the array is sealed with silicone, which is water permeable (Donaldson 1991). While water itself is not conductive, ions on the array surface mobilized

by infiltrating water could create conductive bridges across electrodes. In addition, parylene delamination and cracking along the electrode shafts (Schmidt *et al* 1988, Loeb *et al* 1977) or failure of critical parylene–silicone junctions could produce shunting of neural signals, thereby reducing their amplitude over time. In a more limited sample, using scanning electron microscopy, Schmidt *et al* (1988) demonstrated that parylene cracking and delamination can give rise to the same correlated drop in impedance and lower signal quality that we observed. In our study, early arrays were sterilized using high-temperature steam sterilization which makes parylene more brittle and predisposed to cracking (Hassler *et al* 2010), but the majority of our implants were gas sterilized (EtO), thus reducing concerns that this was the major source of material failure in our results. Differing responses across and within electrodes may account for the large amount of variability observed across the data set. Caution is warranted in extending this conclusion. Substantial differences in size, shape, coating material and thickness, insertion technique, surgical procedure, manufacturing venue (lab or commercial), quality control, and species could have profound effects on local tissue and material responses and recording quality both acutely and over time. Our conclusion predicts that intraparenchymal responses are not important contributors to failure over the long term, but histological evaluations, not reported here in our study, would help to further establish this point. It is also important to note that materials failure is likely to be a function of the complex tissue milieu, and is thus tied to biological responses. Local cell products, especially oxygen species, could degrade materials (Potter *et al* 2013, Patrick *et al* 2011). The effect of tissue response on electrode material integrity requires further investigation. Our results indicate that material shortcomings could be overcome either by better, more resistant biomaterials or by agents that suppress elements in the tissue that attack materials, or both. In either case, these solutions should lead to sensors capable of recording for many years.

**5.3.1. Meningeal responses—**Meningeal encapsulation accounted for more than half of chronic failures (figures 7 and 8), where undergrowth as well as overgrowth extracted the MEA from the cortex. While all implants showed some degree of meningeal thickening (as grossly observed), it was clearly not always sufficient to extract the electrode since recordings continued. Extraparenchymal responses are often ignored as a failure mode. The growth of infiltrating fibroblasts from the arachnoid or dura re-establish the intraparenchymal and extraparenchymal boundary and neurothelial cells of the subdural space generate a glia-limitans like membrane (Shearer and Fawcett 2001). Progressive meningeal growth that gradually lifts the array out of the cortex could explain some of the slow decline in signal amplitude, but this would not account for impedance drops. It is not clear why this reaction occurs or what factors determine why it varies substantially in form across monkeys. Array implantation across a sulcus, over a pial vessel where arachnoid is thickened, or through existing scar tissue may play a role. Subdural Teflon placement has been employed to inhibit meningeal reactions (Maynard *et al* 2000), but our data does not support the value of that approach. Encapsulation tissue was found on arrays with and without subdural Teflon (figure 7(e)). Steroids may help to control this response (Zhong and Bellamkonda 2007), but this has not been tested for our arrays. Further research on the mechanism of meningeal encapsulation is necessary in order to understand and control this

response and to determine whether similar responses could be present in human brain implants.

### 5.4. Signal instability

Another important mechanical factor not directly addressed here is the micro-motion of the array in the brain. A mismatch in the modulus of elasticity between a rigid array and neural tissue may also be a source of micro-motion (Lee *et al* 2005). Further, pulling on the spring-like cable that attaches the array to the pedestal or motion of the array itself, even at the level of tens of microns can produce signal instabilities as the sensor tip moves slightly, potentially detecting a different neuron. The day-to-day variability in the number of signals typically recorded on these arrays supports this view, as previously reported (Suner *et al* 2005, Chestek *et al* 2011).

### 5.5. Improving recording reliability

Taking all of these results together, our data indicate that a number of causes contribute to unreliable long-term recording and electrode failure. Our classification system for the multiple time scales and causes of failure provides a basis for comparison intended to facilitate improvements in device design and recording quality. Using this structure we can make several recommendations for advancement. Careful surgical procedures and fastidious wound care are essential. For humans, of course, these factors are much more reliably controlled and not as problematic as in NHPs. The currently used connector is also a concern because it is a mechanical lever point and it requires a breach in the skin, which is a potential route for infection. A wireless, fully implantable device would eliminate these issues. Fully implantable systems capable of transmitting the full bandwidth of signals from this array are already in initial animal testing (Borton *et al* 2013). A more flexible cable from the array to the pedestal (or wireless module) could improve mechanical stability on the micro-scale and would facilitate implantation. Our data also suggests that a new perspective on tissue reaction be adopted, at least for this sensor and its current applications. While it is certain that many tissue responses occur when the array is implanted and left in place, it appears as if gliosis, cell death, vascular damage and other tissue responses have little impact on recording quality, at least that is presently measurable.

High quality recordings (based on amplitude, number of viable channels, and SNR) were obtained throughout the period of maximum tissue response, and this is true for the early stages of recording in humans as well (Truccolo *et al* 2011). On the other hand, our evidence suggests that tissue responses are likely to be important contributors in degrading materials necessary to maintain the integrity of the sensor's electrical pathway. Drops in signal amplitude, noise, and impedance over time support this hypothesis. The nature of the chemical environment needs to be evaluated both to suppress the response and to make more resistant and secure coatings. The set of responses we see are consistent with biological, mechanical, and materials responses occurring in parallel over the life of the implant. This complex picture has probably accounted for the variety of opinions on the cause(s) of electrode failure. Despite all of these issues, most if not all seem to be readily addressable. The successful recording for many years, already achieved in both NHPs and humans with this sensor (Hochberg *et al* 2012) suggest that decade-long recording sensors are feasible as

these improvements are made. Research that uses metrics such as the ones proposed here to quantify how much these factors limit reliable, stable recording are essential in the ongoing development of long-term neural interfaces for scientific and clinical applications.

## Supplementary Material

Refer to Web version on PubMed Central for supplementary material.

## Acknowledgments

We thank Beth Travers for her help in compiling this enormous data set over the years. We also would like to acknowledge Dr Arto Nurmikko and his colleagues: Juan Aceros, David Borton, Ming Yin, and Shaomin Zhang for their guidance and expertise. A special thanks to Dr James Harper, Veronica Budz, Pamela Norberg, and Roxanne Burrill of the veterinary staff at Brown University for their extraordinary care and compassion. A final thanks to Dr Peter Carmel of the Neurological Institute of New Jersey for his generous financial support.

## References

Bansal AK, Truccolo W, Vargas-Irwin CE, Donoghue JP. Decoding 3D reach and grasp from hybrid signals in motor and premotor cortices: spikes, multiunit activity, and local field potentials. J. Neurophysiol. 2012; 107:1337–1355. [PubMed: 22157115]

Biran R, Martin DC, Tresco PA. Neuronal cell loss accompanies the brain tissue response to chronically implanted silicon microelectrode arrays. Exp. Neurol. 2005; 195:115–126. [PubMed: 16045910]

Bjornsson CS, Oh SJ, Al-Kofahi YA, Lim YJ, Smith KL, Turner JN, De S, Roysam B, Shain W, Kim SJ. Effects of insertion conditions on tissue strain and vascular damage during neuroprosthetic device insertion. J. Neural Eng. 2006; 3:196–207. [PubMed: 16921203]

Borton DA, Yin M, Aceros J, Nurmikko A. An implantable wireless neural interface for recording cortical circuit dynamics in moving primates. J. Neural Eng. 2013; 10:026010. [PubMed: 23428937]

Chestek CA, et al. Long-term stability of neural prosthetic control signals from silicon cortical arrays in rhesus macaque motor cortex. J. Neural Eng. 2011; 8:045005. [PubMed: 21775782]

Collias JC, Manuelidis EE. Histopathological changes produced by implanted electrodes in cat brains; comparison with histopathological changes in human and experimental puncture wounds. J. Neurosurg. 1957; 14:302–328. [PubMed: 13429398]

Donaldson PE. Aspects of silicone rubber as an encapsulant for neurological prostheses: part 1. Osmosis. Med. Biol. Eng. Comput. 1991; 29:34–39. [PubMed: 2016918]

Edell DJ, Toi VV, McNeil VM, Clark LD. Factors influencing the biocompatibility of insertable silicon microshafts in cerebral cortex. IEEE Trans. Biomed. Eng. 1992; 39:635–643. [PubMed: 1601445]

Griffith RW, Humphrey DR. Long-term gliosis around chronically implanted platinum electrodes in the Rhesus macaque motor cortex. Neurosci. Lett. 2006; 406:81–86. [PubMed: 16905255]

Hassler C, von Metzen RP, Ruther P, Stieglitz T. Characterization of parylene C as an encapsulation material for implanted neural prostheses. J. Biomed. Mater. Res. B. 2010; 93:266–274.

Hochberg LR, Serruya MD, Friehs GM, Mukand JA, Saleh M, Caplan AH, Branner A, Chen D, Penn RD, Donoghue JP. Neuronal ensemble control of prosthetic devices by a human with tetraplegia. Nature. 2006; 442:164–171. [PubMed: 16838014]

Hochberg LR, et al. Reach and grasp by people with tetraplegia using a neurally controlled robotic arm. Nature. 2012; 485:372–375. [PubMed: 22596161]

Jones KE, Campbell PK, Normann RA. A glass silicon composite intracortical electrode array. Ann. Biomed. Eng. 1992; 20:423–437. [PubMed: 1510294]

Kim SP, Simeral JD, Hochberg LR, Donoghue JP, Black MJ. Neural control of computer cursor velocity by decoding motor cortical spiking activity in humans with tetraplegia. J. Neural Eng. 2008; 5:455–476. [PubMed: 19015583]

Lee H, Bellamkonda RV, Sun W, Levenston ME. Biomechanical analysis of silicon microelectrode-induced strain in the brain. J. Neural Eng. 2005; 2:81–89. [PubMed: 16317231]

Liu X, McCreery DB, Carter RR, Bullara La, Yuen TG, Agnew WF. Stability of the interface between neural tissue and chronically implanted intracortical microelectrodes. IEEE Trans. Rehabil. Eng. 1999; 7:315–326. [PubMed: 10498377]

Loeb GE, Bak MJ, Salcman M, Schmidt EM. Parylene as a chronically stable, reproducible microelectrode insulator. IEEE Trans. Biomed. Eng. 1977; 24:121–128. [PubMed: 408260]

Maynard EM, Fernandez E, Normann RA. A technique to prevent dural adhesions to chronically implanted microelectrode arrays. J. Neurosci. Methods. 2000; 97:93–101. [PubMed: 10788663]

Maynard EM, Hatsopoulos NG, Ojakangas CL, Acuna BD, Sanes JN, Normann RA, Donoghue JP. Neuronal interactions improve cortical population coding of movement direction. J. Neurosci. 1999; 19:8083–8093. [PubMed: 10479708]

McConnell GC, Rees HD, Levey AI, Gutekunst C-A, Gross RE, Bellamkonda RV. Implanted neural electrodes cause chronic, local inflammation that is correlated with local neurodegeneration. J. Neural Eng. 2009; 6:056003. [PubMed: 19700815]

Mercanzini A, Colin P, Bensadoun JC, Bertsch A, Renaud P. *In vivo* electrical impedance spectroscopy of tissue reaction to microelectrode arrays. IEEE Trans. Biomed. Eng. 2009; 56:1909–1918. [PubMed: 19362904]

Merrill DR, Tresco PA. Impedance characterization of microarray recording electrodes. in vitro Proc. IEEE Annu. Int. Conf. Engineering in Medicine and Biology Society. 2004; 6:4349–4352.

Patrick E, Orazem ME, Sanchez JC, Nishida T. Corrosion of tungsten microelectrodes used in neural recording applications. J. Neurosci. Methods. 2011; 198:158–171. [PubMed: 21470563]

Polikov VS, Tresco PA, Reichert WM. Response of brain tissue to chronically implanted neural electrodes. J. Neurosci. Methods. 2005; 148:1–18. [PubMed: 16198003]

Potter KA, Buck AC, Self WK, Callanan ME, Sunil S, Capadona JR. The effect of resveratrol on neurodegeneration and blood brain barrier stability surrounding intracortical microelectrodes. Biomaterials. 2013; 34:7001–7015. [PubMed: 23791503]

Prasad A, Sanchez JC. Quantifying long-term microelectrode array functionality using chronic *in vivo* impedance testing. J. Neural Eng. 2012; 9:026028. [PubMed: 22442134]

Rousche PJ, Normann RA. A method for pneumatically inserting an array of penetrating electrodes into cortical tissue. Ann. Biomed. Eng. 1992; 20:413–422. [PubMed: 1510293]

Rousche PJ, Normann RA. Chronic recording capability of the Utah intracortical electrode array in cat sensory cortex. J. Neurosci. Methods. 1998; 82:1–15. [PubMed: 10223510]

Saxena T, Karumbaiah L, Gaupp EA, Patkar R, Patil K, Betancur M, Stanley GB, Bellamkonda RV. The impact of chronic blood-brain barrier breach on intracortical electrode function. Biomaterials. 2013; 34:4703–4713. [PubMed: 23562053]

Schmidt EM, McIntosh JS, Bak MJ. Long-term implants of Parylene-C coated microelectrodes. Med. Biol. Eng. Comput. 1988; 26:96–101. [PubMed: 3199908]

Schmitt G, Schultze JW, Fassbender F, Buss G, Luth H, Schoning MJ. Passivation and corrosion of microelectrode arrays. Electrochim. Acta. 1999; 44:3865–3883.

Schultz RL, Willey TJ. The ultrastructure of the sheath around chronically implanted electrodes in brain. J. Neurocytol. 1976; 5:621–642. [PubMed: 1003257]

Shearer MC, Fawcett JW. The astrocyte/meningeal cell interface—a barrier to successful nerve regeneration? Cell Tissue Res. 2001; 305:267–273. [PubMed: 11545264]

Suner S, Fellows MR, Vargas-Irwin C, Nakata GK, Donoghue JP. Reliability of signals from a chronically implanted, silicon-based electrode array in non-human primate primary motor cortex. IEEE Trans. Neural Syst. Rehabil. Eng. 2005; 13:524–541. [PubMed: 16425835]

Szarowski DH, Andersen MD, Retterer S, Spence AJ, Isaacson M, Craighead HG, Turner JN, Shain W. Brain responses to micro-machined silicon devices. Brain Res. 2003; 983:23–35. [PubMed: 12914963]

Truccolo W, Donoghue JA, Hochberg LR, Eskandar EN, Madsen JR, Anderson WS, Brown EN, Halgren E, Cash SS. Single-neuron dynamics in human focal epilepsy. Nature Neurosci. 2011; 14:635–641. [PubMed: 21441925]

Turner JN, Shain W, Szarowski DH, Andersen M, Martins S, Isaacson M, Craighead H. Cerebral astrocyte response to micromachined silicon implants. Exp. Neurol. 1999; 156:33–49. [PubMed: 10192775]

Williams JC, Hippensteel JA, Dilgen J, Shain W, Kipke DR. Complex impedance spectroscopy for monitoring tissue responses to inserted neural implants. J. Neural Eng. 2007; 4:410–423. [PubMed: 18057508]

Yuen TG, Agnew WF, Bullara LA. Tissue response to potential neuroprosthetic materials implanted subdurally. Biomaterials. 1987; 8:138–141. [PubMed: 3555632]

Zhong Y, Bellamkonda RV. Dexamethasone-coated neural probes elicit attenuated inflammatory response and neuronal loss compared to uncoated neural probes. Brain Res. 2007; 1148:15–27. [PubMed: 17376408]

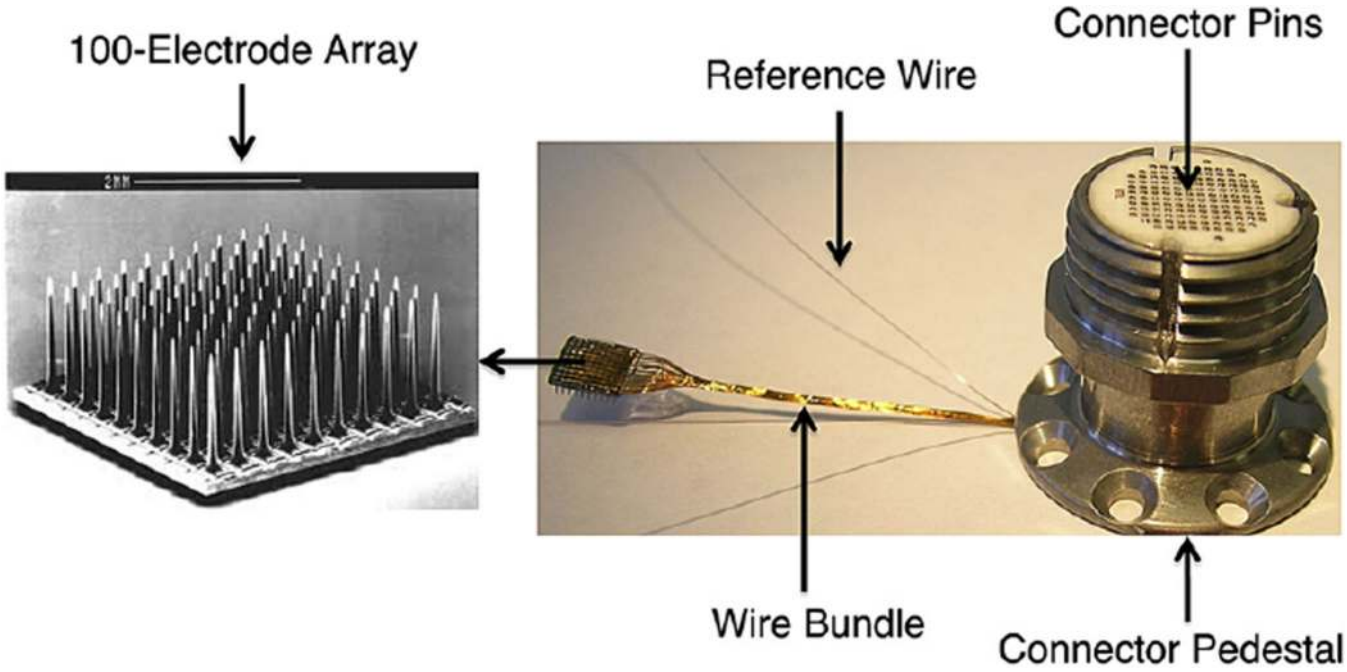


**Figure 1.**

Silicon MEA with CerePort connector. *Left*: Scanning electron micrograph of a 100-electrode array. *Right*: Bundle of 96 wires running to Ti pedestal connector, which is secured to the skull using titanium screws. The connector pads mate to a spring-pin loaded 'patient cable' connector that screws onto the pedestal and delivers signals to a preamplifier (See Cerebus® Neural Signal Processing System: User's Manual, revision 13.0). The implant has two common signal reference wires, placed in the recording field (usually subdural).

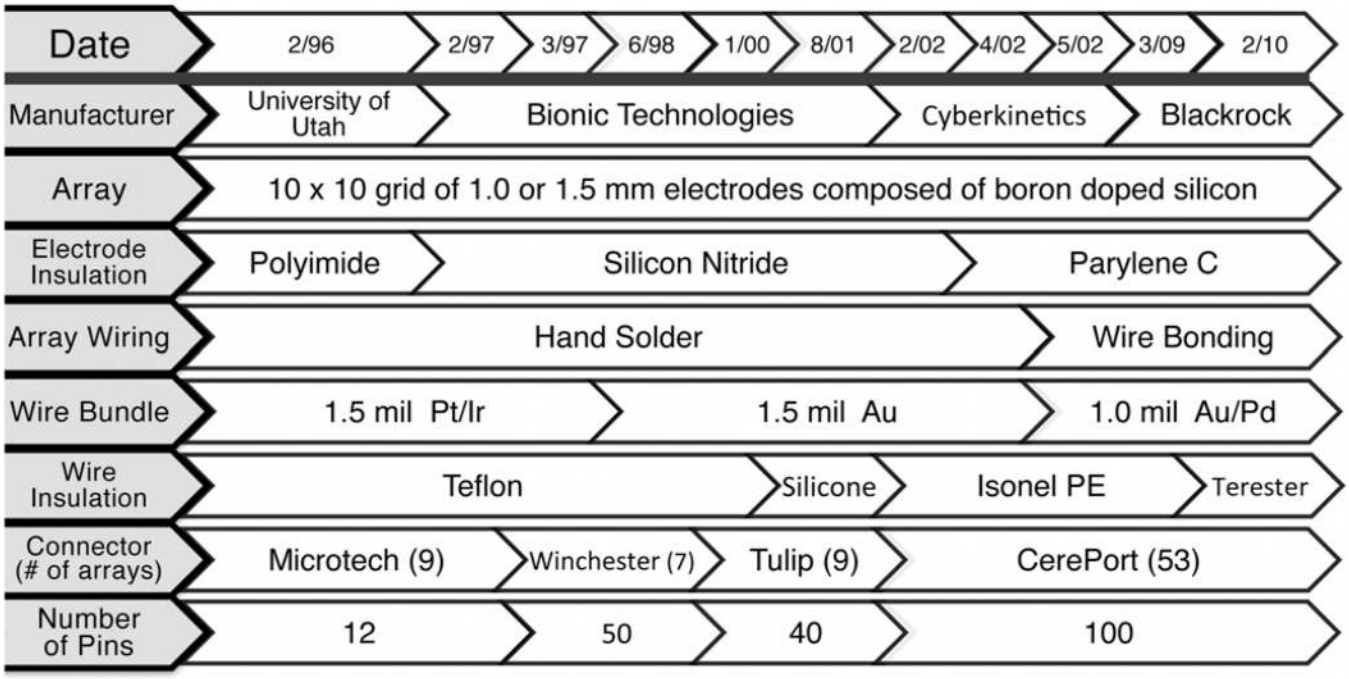


**Figure 2.**

Developmental process of the 'Utah' array. This table summarizes the approximate dates at which each design feature was implemented beginning with arrays fabricated in the Normann Laboratory at the University of Utah, then later by commercial entities (Bionic, Cyberkinetics, and Blackrock). Note that the form of the array has remained the same, but insulation, fabrication methods, wire bundle composition, connector type and number of possible connections have been modified over the years.

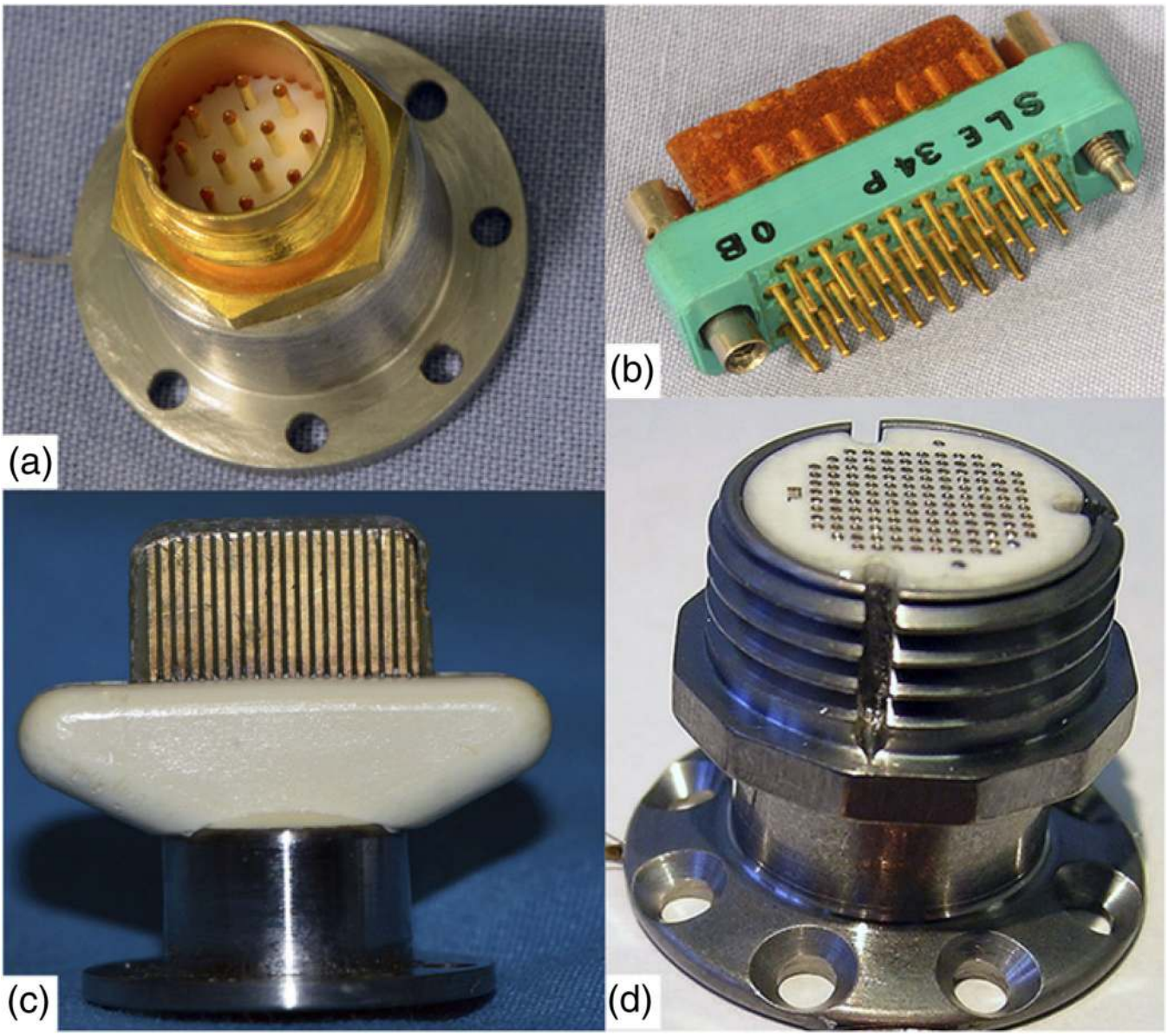


**Figure 3.**

Types of connectors used across this study arranged according to their history of use. (a) Initial Microtech connector with 12 pins. (b) Winchester style connector with 34 pins. (c) Tulip connector with 40 pins. (d) Current CerePort connector with 100 functional contact pads.

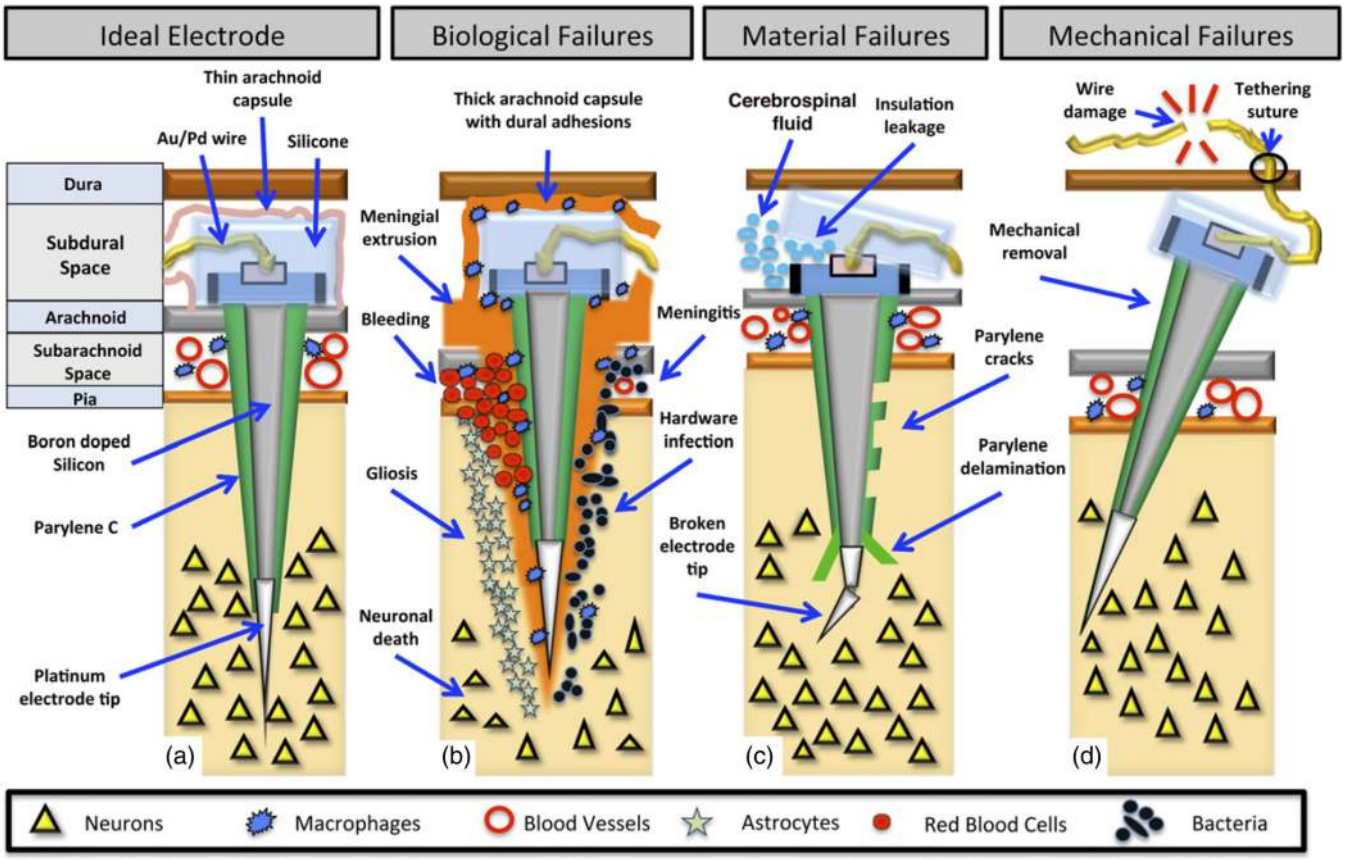


**Figure 4.**

Major failure modes of MEAs. (a) Ideal placement in cortical tissue, about 1 (or 1.5) mm into the cortex. A thin layer of arachnoid overgrowth encases the platform that sits on the pia-arachnoid surface and helps to stabilize the array. (b) Biological failures: bleeding, cell death, hardware infection, meningitis, gliosis, or meningeal encapsulation and extrusion. Macrophages originating in the subarachnoid space may mediate the encapsulation response. (c) Material failures: broken electrode tips, insulation leakage, or parylene cracks and delamination. Note that the latter three would lead to lower impedances and spike amplitudes due to shunting. (d) Mechanical failures: wire bundle damage, connector damage, and mechanical removal. A dural stitch is shown as one possible source of tethering that results in electrodes being pulled out of the brain.

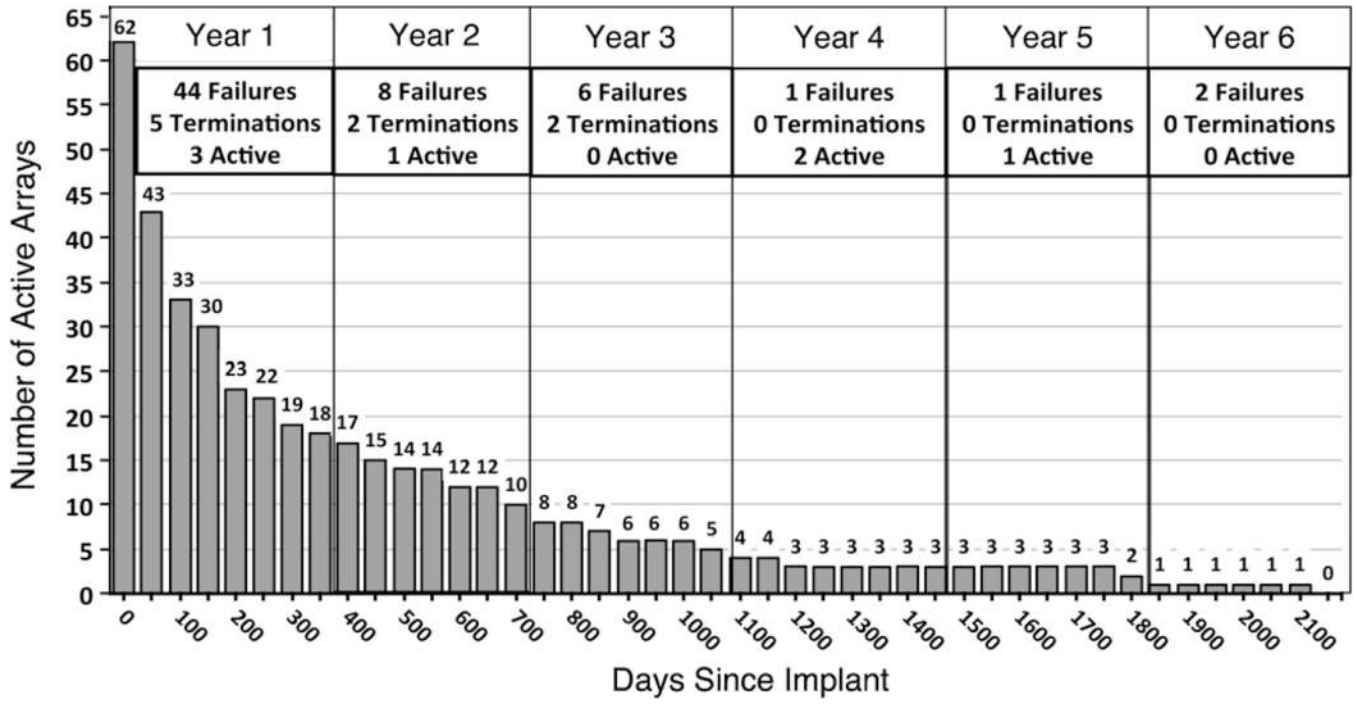


**Figure 5.**

Array time to failure. All array durations are aligned to the time of implantation. This chart shows how many of the failed arrays ($n = 62$) remained active at 50-day intervals from implantation. A yearly summary of all array ($n = 78$) outcomes is presented in the boxes along the top of the chart. The yearly summaries account for the arrays that were electively terminated ($n = 9$) or remained active ($n = 7$) at the close of this study.

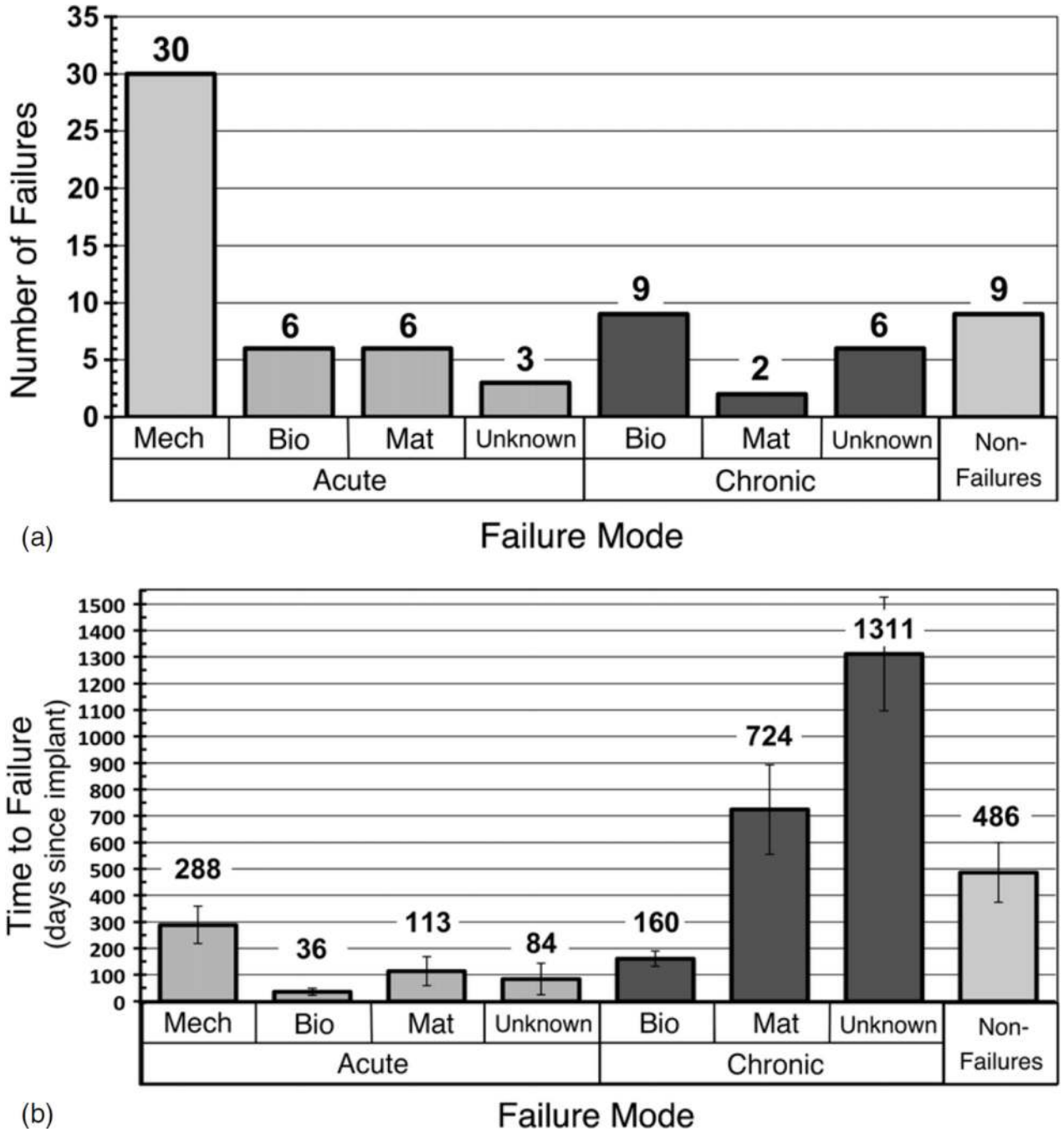


**Figure 6.**

Failures by mode. (a) This chart shows the number of arrays that failed by each failure mode category. Note that acute mechanical failures were most common. (b) This chart shows the mean time to failure for each class of failure modes. Error bars indicate the sem. Note that the chronic unknown failure category had the longest mean time to failure.

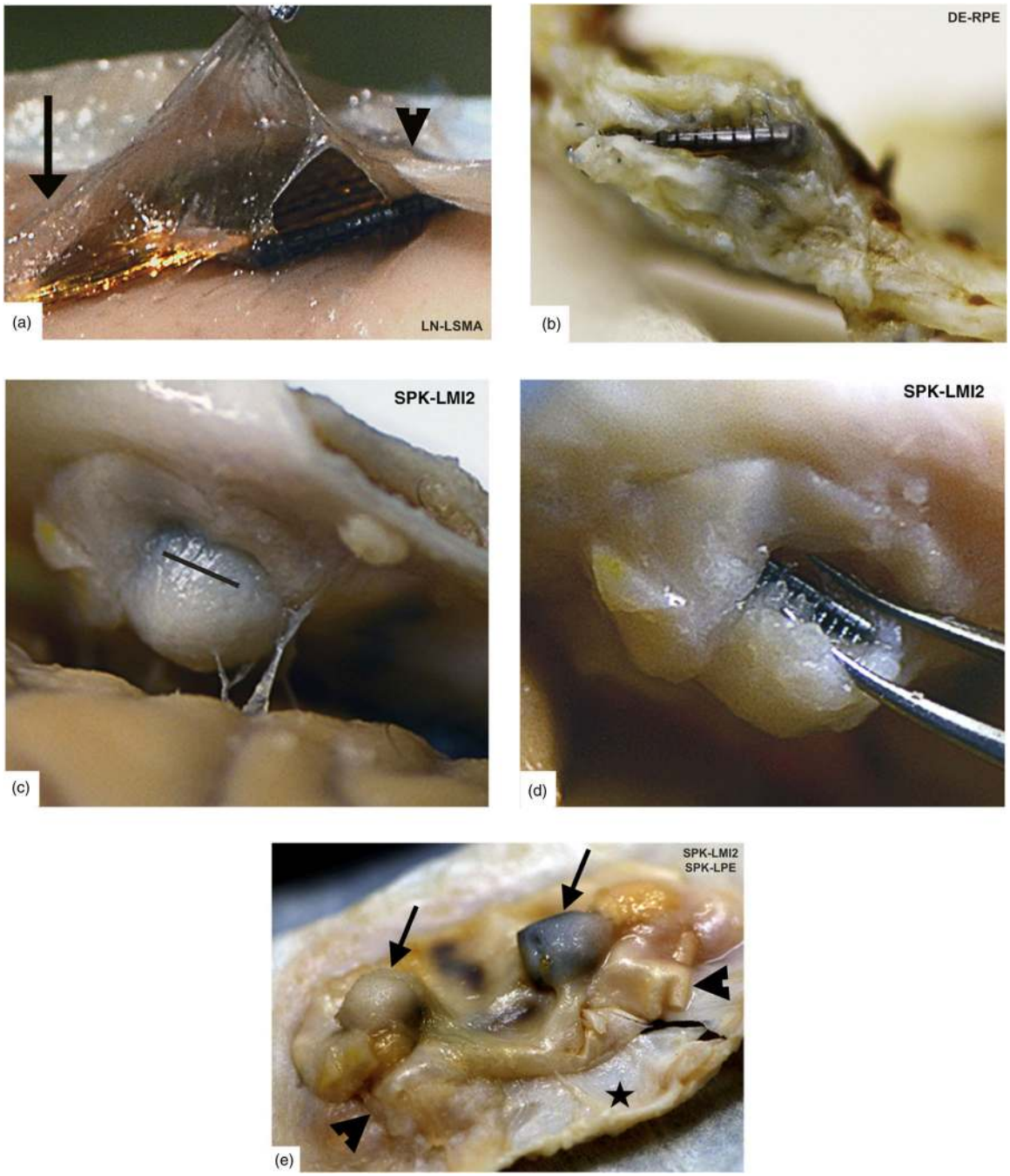


**Figure 7.**

Encapsulated arrays–gross specimens. All of our arrays showed grossly visible encapsulation, however the extent of encapsulation varied greatly. (a) Thin tissue capsule with arachnoid appearance at 37 days post-implant. This tissue can be seen merging with normal arachnoid to the left (arrow) and normal dura to the right (arrowhead). (b) Dense fibrous tissue encapsulation at 761 days post-implant. The array is intradural in this photo. (c) Complete encapsulation by day 853. The capsule was cut open (black line) in order to visualize the array seen in (d). (e) Two arrays with varying degrees of thick encapsulation

tissue (arrows) under each array at 853 days (viewed from below). A Teflon layer (Gore® Preclude® Dura Substitute, WL Gore and Associates, Flagstaff, AZ) was placed above the array and below the dura during implantation to prevent encapsulation. This photo indicates that subdural Teflon does not prevent encapsulation and extrusion, as the Teflon sheet was also encapsulated. Arrowheads indicate its location between the fibrous tissue capsule and the adjacent dura (black star). (Array names reflect monkey name and implant location).

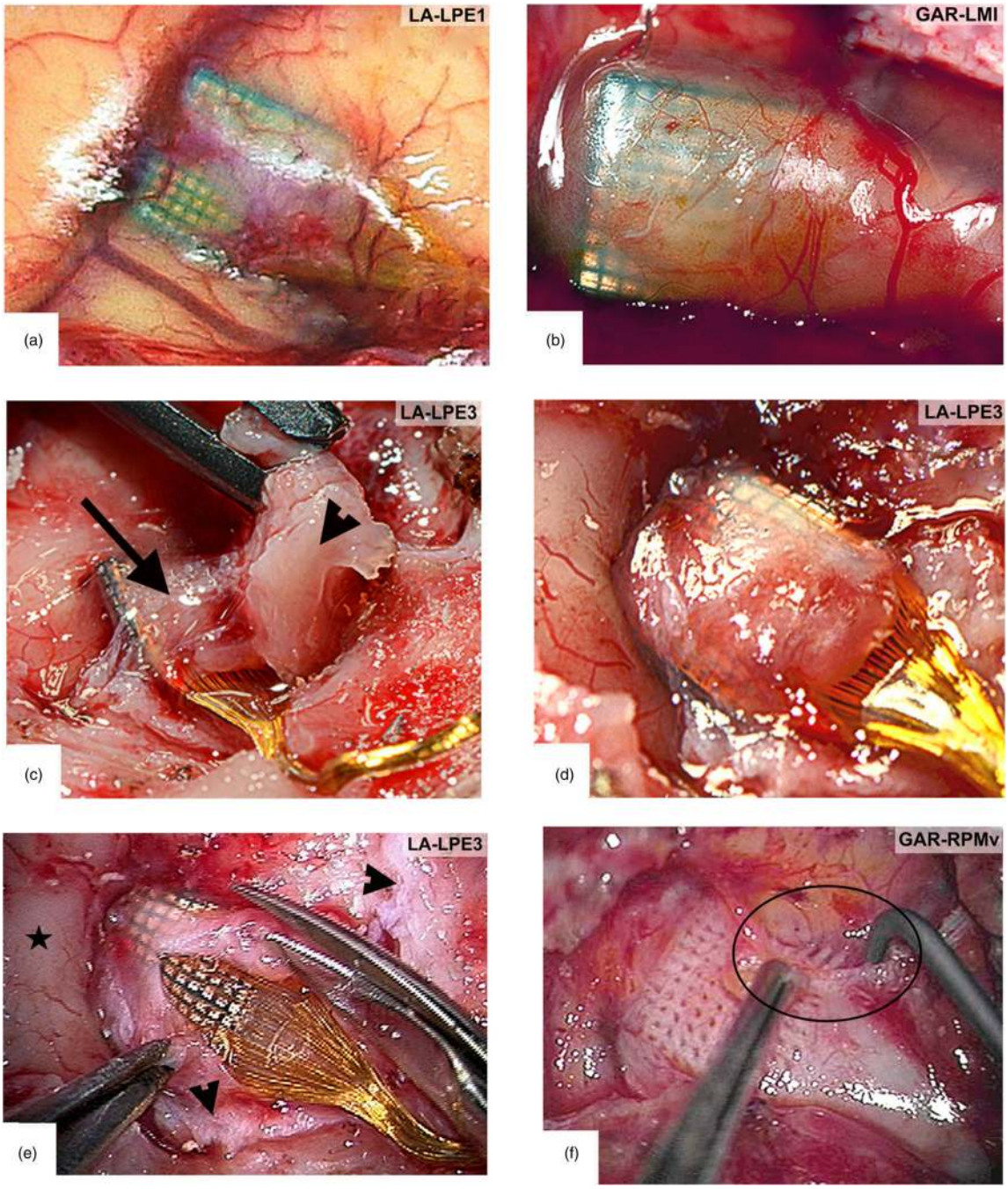


**Figure 8.**

Encapsulated arrays –intra-operative specimens. (a) Thin arachnoid encapsulation tissue with prominent neovascularization over the top of an array at 264 days post-implant. The dura was reflected with minimal adherence to this tissue. (b) An array explanted at 765 days post-implant with a slightly thicker arachnoid encapsulation, but no dural adhesions. (c) Surgical removal of dura (arrowhead) adherent to the arachnoid encapsulation (arrow) of an array at 1051 days post-implant. (d) The arachnoid encapsulation after dura has been removed. Note how the cortex is depressed at the implant site. (e) Microsurgical dissection

of the same arachnoid capsule from (d) as seen through an operating microscope. Normal cortex (covered with normal arachnoid) is indicated by the black star. Dura is indicated at the borders by arrowheads. (f) After removing the array, a thickened arachnoid layer is observed below the array with a grid-like pattern caused by the individual electrodes. The picture shown, however, is from a different monkey explanted at 554 days with nearly identical findings. This photo shows that as the floor of the capsule is gently pulled aside, additional meningeal encapsulation tissue can be seen along the electrode tracts, diving down into the cortex (black circle). (Array names reflect monkey name and implant location.)

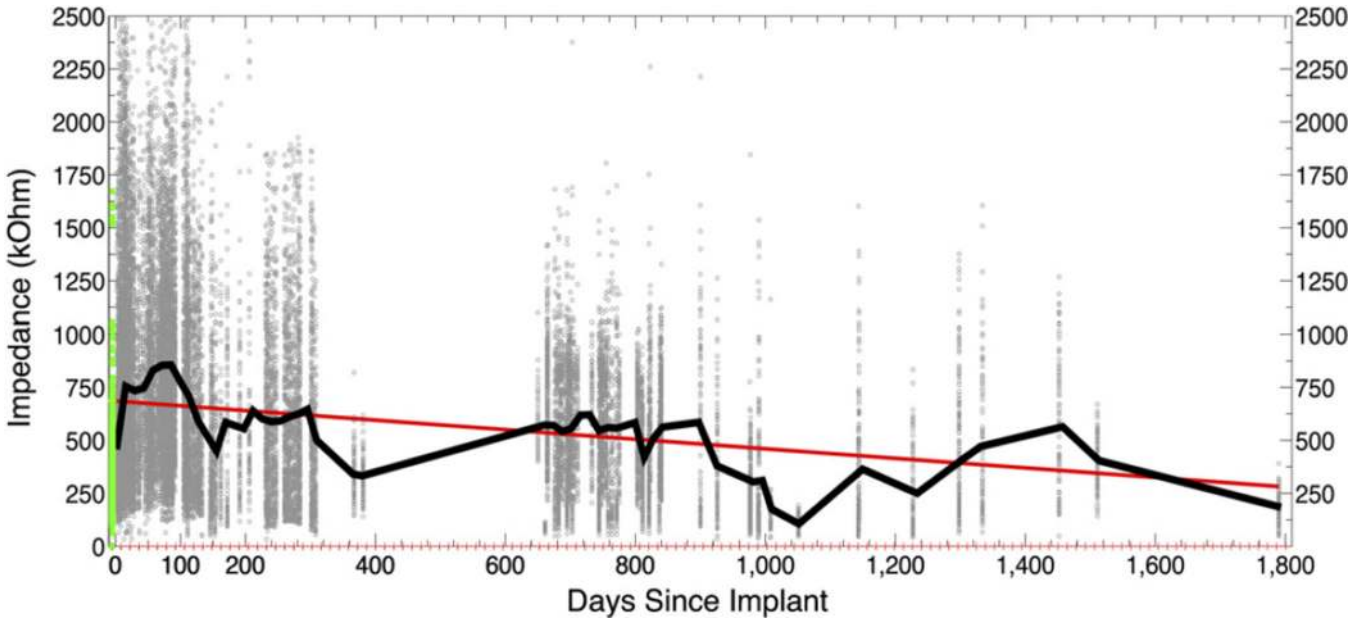


**Figure 9.**

Impedance over time. Every 1 kHz impedance value (<2500 kΩ) for 26 arrays across 305 sessions is shown as a scatter plot (background dots, $n$= 29 280). The green points represent all pre-implant impedances as reported by the manufacturer. The black line plots the mean impedance value across all arrays per 14-day bin. Red ticks along the $x$-axis indicate bin margins. The red line is the linear regression fit ($y = -0.23x + 6.9e + 002$).

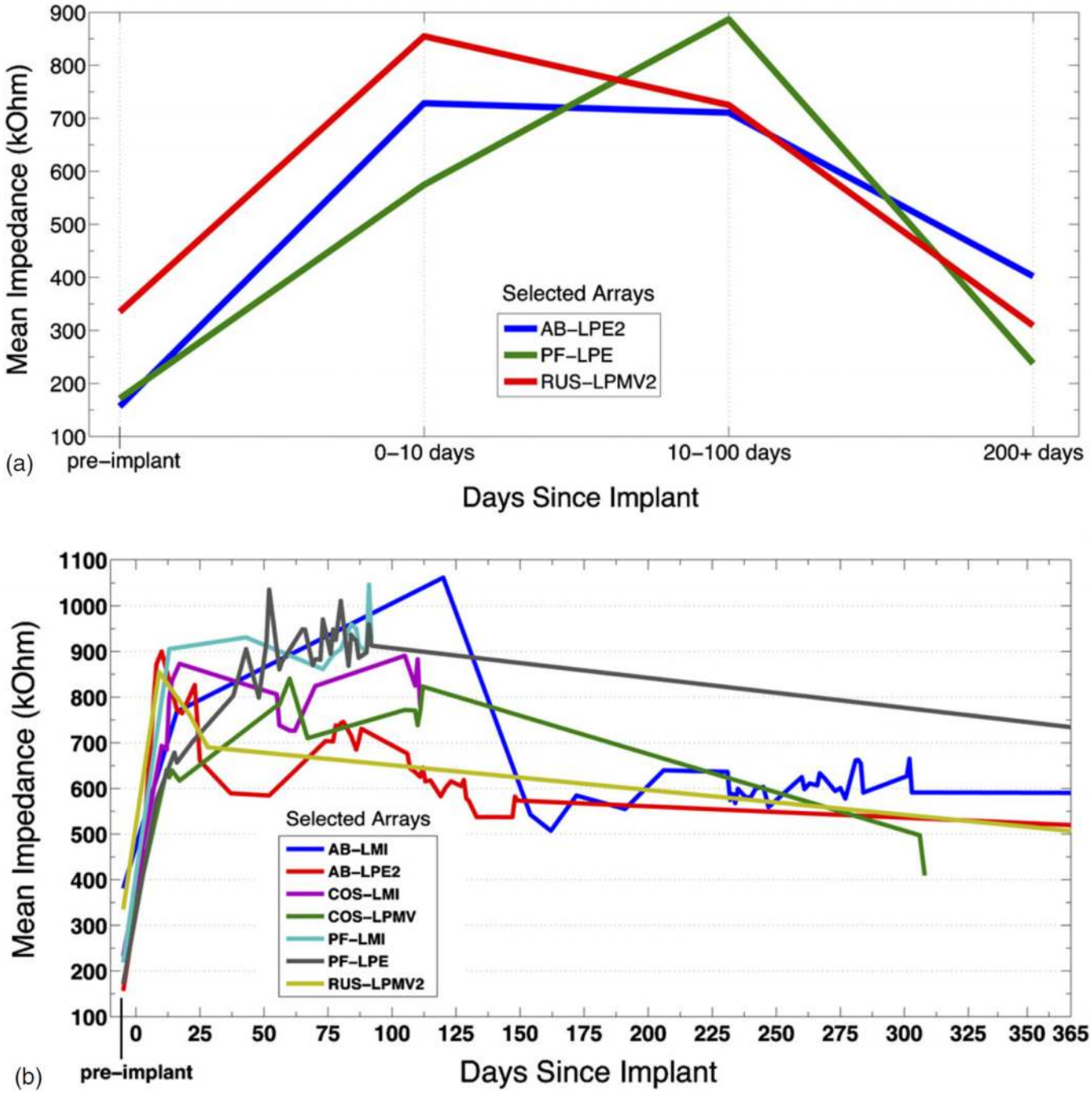


**Figure 10.**

Selected impedance trends. (a) Three arrays with abundant short- and long-term impedance data. The recording sessions were divided into pre-implant values, immediate post-implant values (0–10 days), 3-month post-implant values (10–100 days), and long-term values (200–1000 days). The mean impedance at each session for each array was calculated and the mean across all sessions (per epoch) for each array was plotted. Impedances rise about three-fold in the first ten days after implantation, plateau over the next 3–4 months, then fall steadily over time. The cause of these changes may be independent and are not revealed by this plot.

(b) Seven arrays with abundant impedance data over the first year since implant. The mean impedance for each array at each session is plotted. These results demonstrate that the global trends seen across all arrays reflect individual trends as well. Impedances rise dramatically in the first 10 days after implantation, plateau for the next 100 days, then drop. The rate of decay seems to slow after 200 days. (Array names reflect monkey name and implant location.)

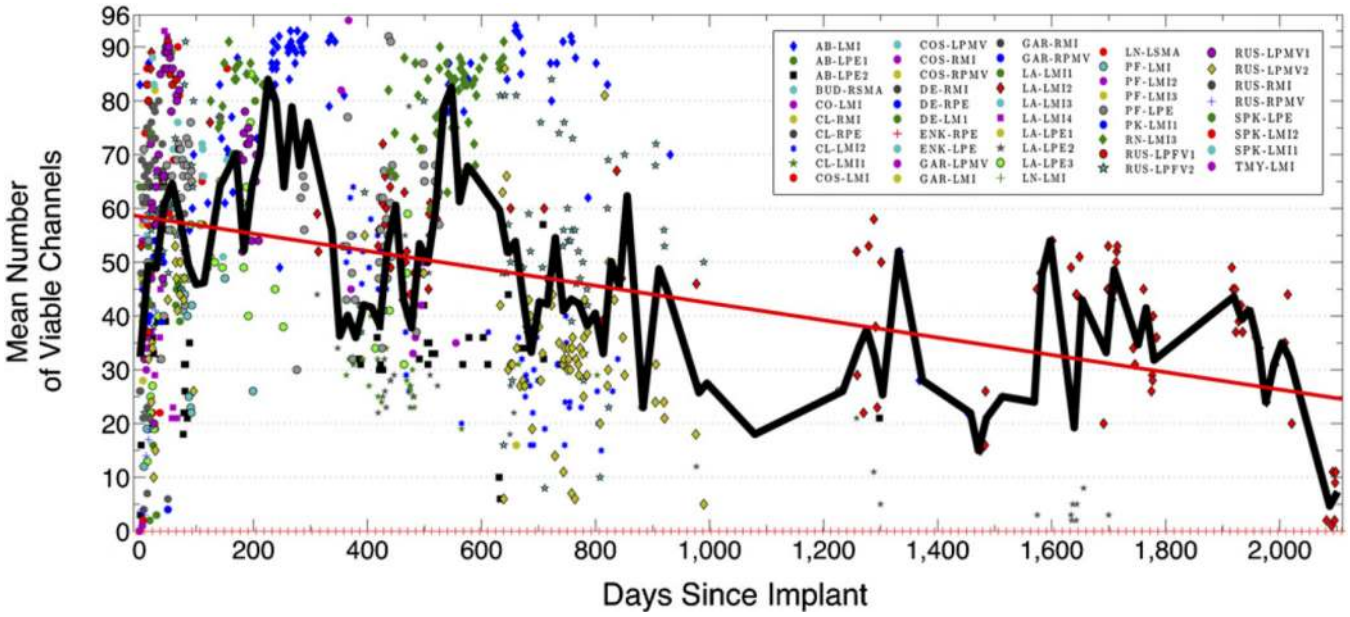


**Figure 11.**

Viable channels over time. The number of viable channels per array at each recording session for 47 CerePort arrays is shown as a scatter plot (colored dots). A different color and/or shape marker represents each array (see legend). The black line is the mean value across all arrays per 14-day bin. Red ticks along the *x*-axis indicate bin margins. The red line shows the linear regression ($y = -0.016x + 59$). The total number of data points (recording sessions) is $n = 1073$. (Array names reflect monkey name and implant location.)

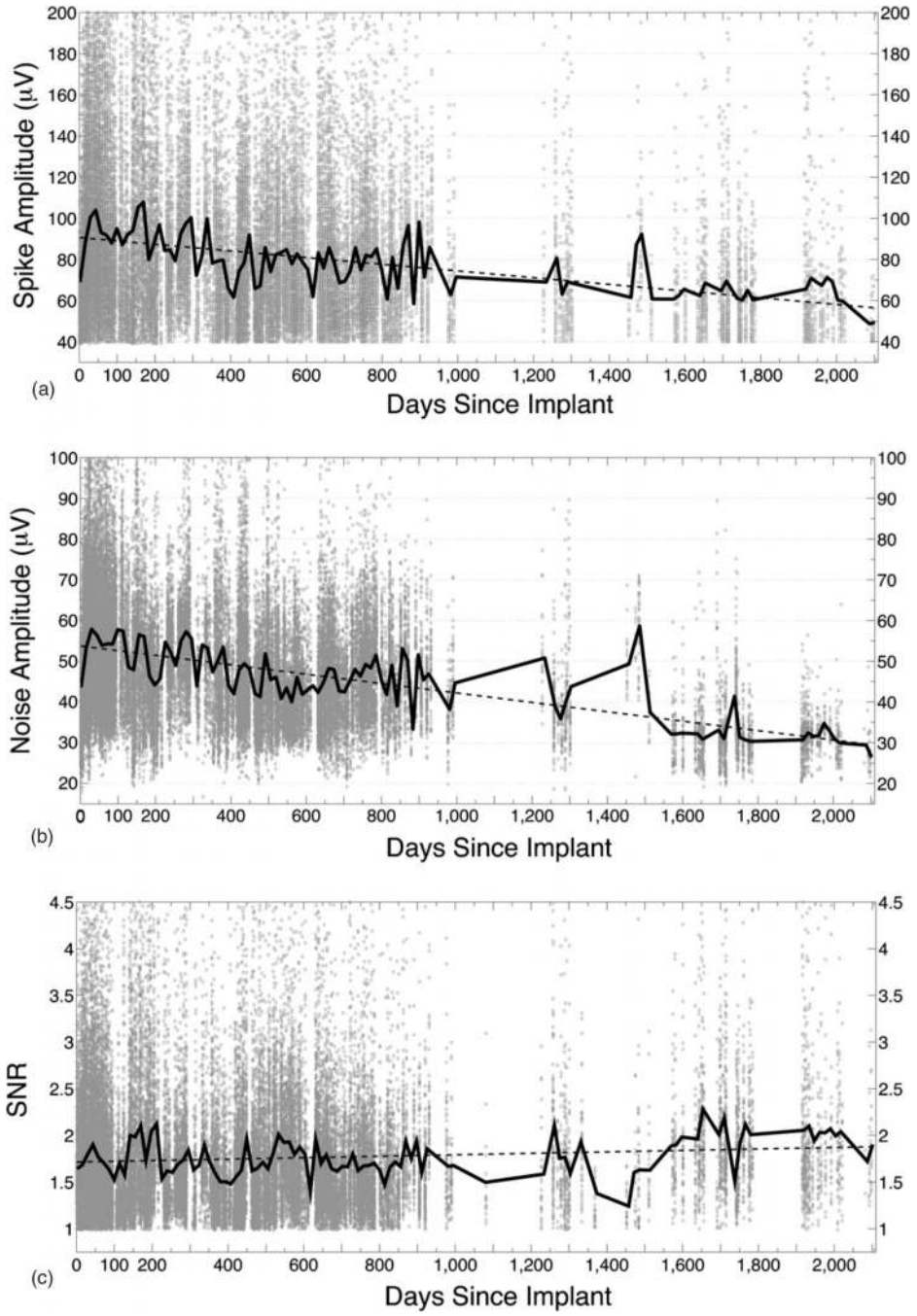


**Figure 12.**

Signal quality over time. (a) Spike amplitude of viable channels over time. The spike amplitude (PTP) per viable channel per array at each recording session for 47 arrays is shown as a scatter plot (background dots, $n = 103\ 008$). The black line is the mean value across all arrays per 14-day bin. The dotted line is the linear regression ($y = -0.017x + 91$). Note that spike amplitude is not predicted by the impedance (figure 9). (b) Noise amplitude of viable channels over time. The noise amplitude per channel per array at each recording session for 47 arrays is shown as a scatter plot (background dots, $n = 103\ 008$). The black

line is the mean value across all arrays per 14-day bin. The dotted line is the linear regression ($y = -0.012x + 54$). Note that the noise amplitude drops at a similar rate as the spike amplitude. (c) SNR of viable channels over time. The SNR per channel per array at each recording session for 47 arrays is shown as a scatter plot (background dots, $n = 103\,008$). The black line is the mean value across all arrays per 14-day bin. The dotted line is the linear regression ($y = 7.8e{-}005x + 1.7$).

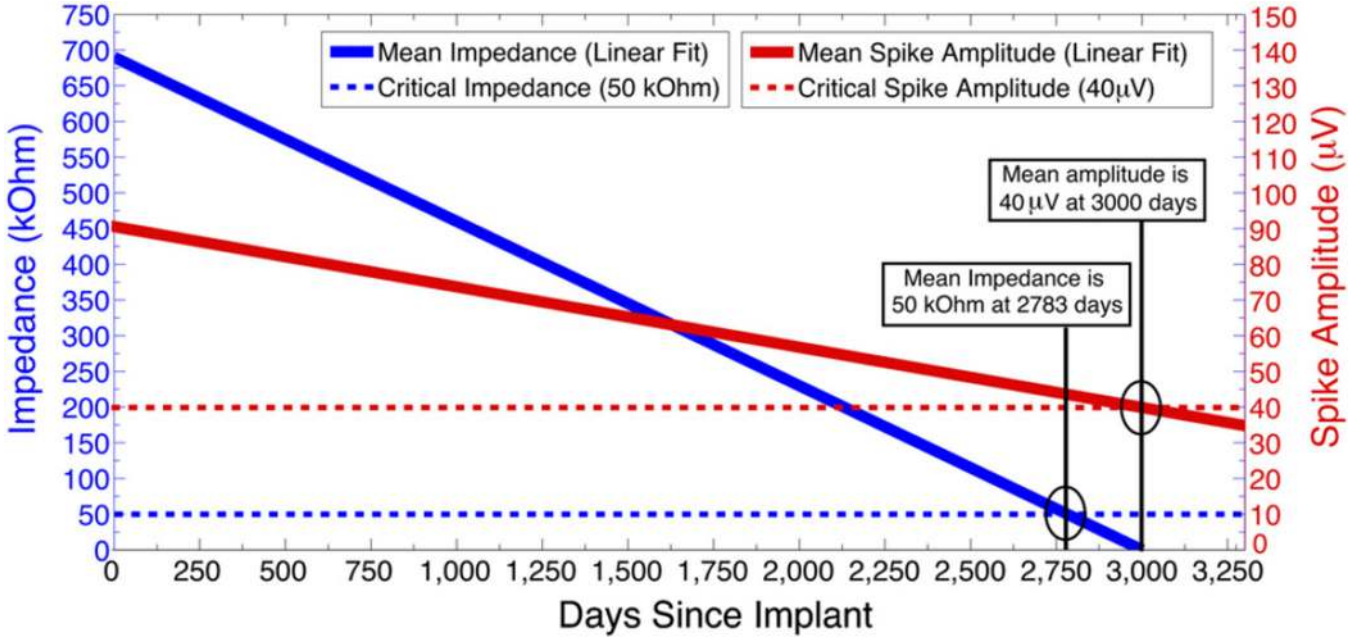


**Figure 13.**

Rates of signal decay. This graph overlaps linear regression models for impedance and spike amplitude (PTP), in order to compare their intercepts (note that slopes cannot be compared because axes are different). Critical values (empirically derived) where the system has failed are plotted as dashed lines. Thus, mean impedance values that degrade to <50 kΩ suggest that signals are largely shunted to ground; spikes with amplitudes <40 μV are effectively impossible to separate from background noise. The different *y* intercepts could suggest multiple, interacting failure modes but the data suggest that the technology could function for up to eight years.

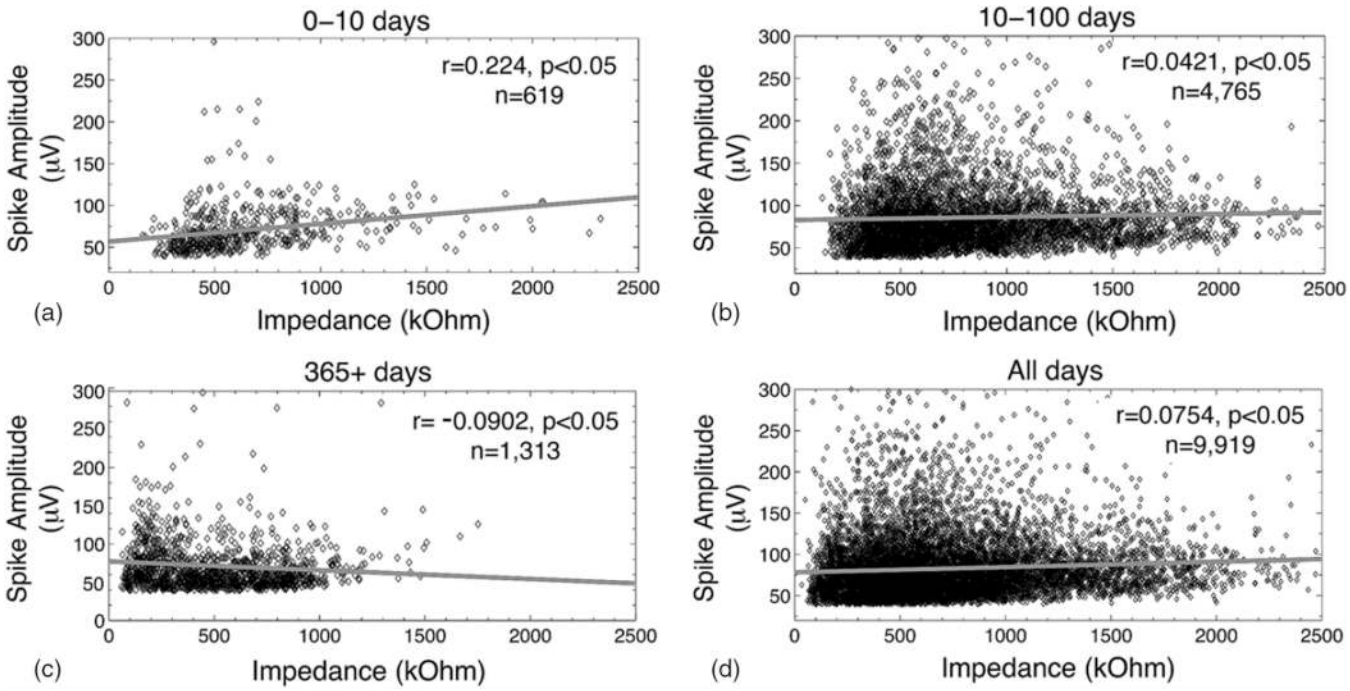


**Figure 14.**

Correlation between spike amplitude and impedance. All recording sessions with concurrent impedance measurements and spike amplitudes were compiled ($n = 104$). The data was then divided into four groups: (a) immediate post-implant values (0–10 days), (b) 3-month post-implant values (10–100 days), (c) long-term values (365 + days), and (d) all values. For each data subset, a correlation coefficient was calculated. The total number of data points is 9919. A very small, significant, positive correlation was found at all time points except for the long-term, where a small, but significant, negative correlation was found. These results suggest that multiple factors beyond impedance determine signal quality.

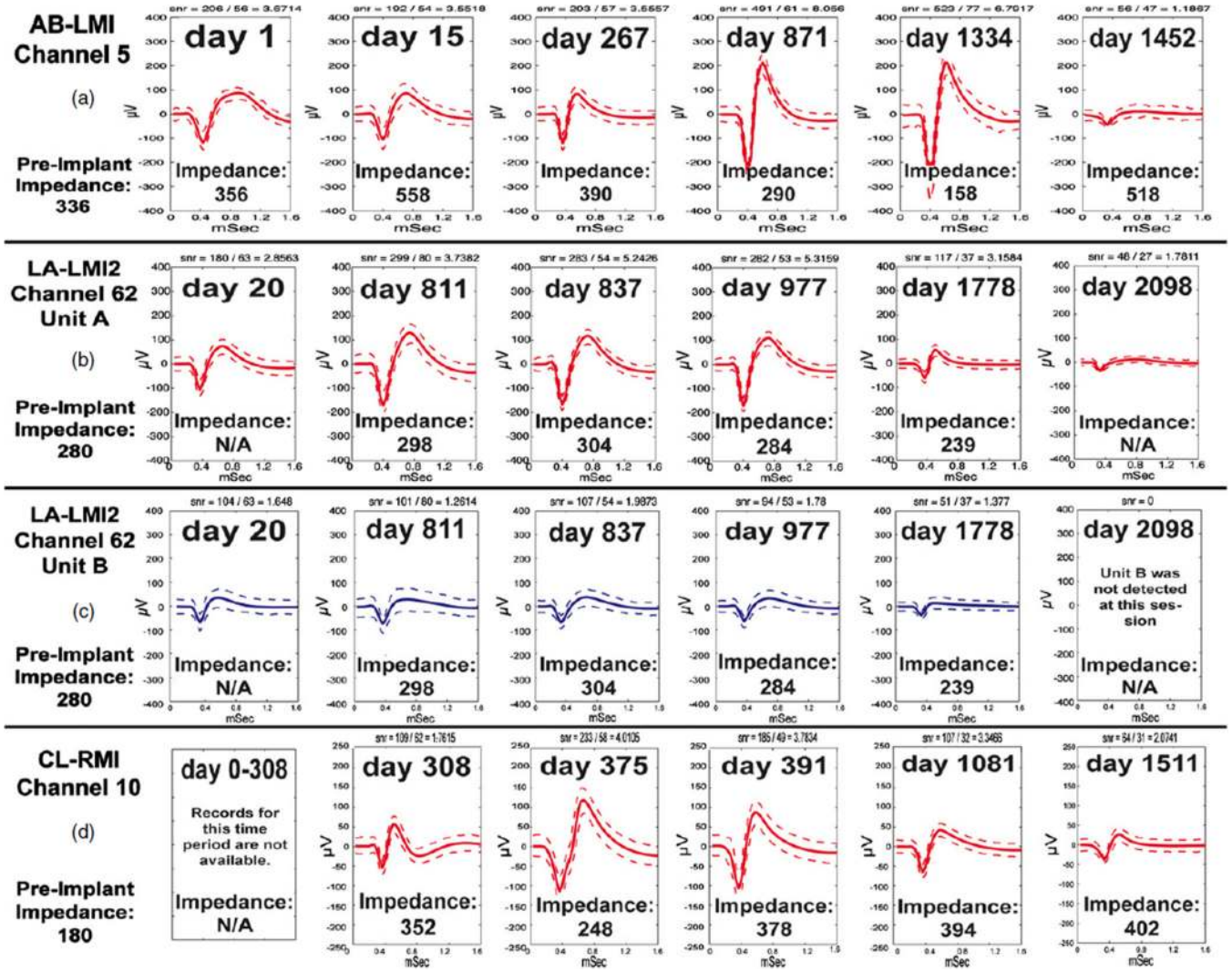


**Figure 15.**

Recording quality of selected channels over time. (a) A channel showing spike recordings where shape and amplitude vary in size at different times, without a clear trend in any direction. (b) One of two units on a selected channel from the longest lasting array. Spikes were evident and impedances were stable for over four years. (c) A second, smaller unit on the same channel from (b). Note different trends in amplitude changes, except that the last recordings in every case had the smallest waveforms. (d) A third long-term array, showing a decline in signal amplitude for this channel despite stable impedances. (Array names reflect monkey name and implant location.)

**Table 1**

Array duration statistics (in days since implant).

| | All arrays | Active arrays | Non-failures | Failed arrays | Biological | | Mechanical | | Material | | Unknown | |
|---|---|---|---|---|---|---|---|---|---|---|---|---|
| | | | | | Acute | Chronic | Acute | Chronic | Acute | Chronic | Acute | Chronic |
| No. of arrays | 78 | 7 | 9 | 62 | 6 | 9 | 30 | 0 | 6 | 2 | 3 | 6 |
| Min | 0 | 104 | 37 | 0 | 3 | 21 | 0 | N/A | 0 | 555 | 0 | 690 |
| Max | 2104 | 1539 | 994 | 2104 | 74 | 261 | 1832 | N/A | 341 | 893 | 198 | 2104 |
| Mean | 387 | 753 | 486 | 332 | 36 | 160 | 288 | N/A | 113 | 724 | 84 | 1311 |
| Median | 182 | 748 | 310 | 133 | 30 | 163 | 130 | N/A | 67 | 724 | 54 | 1146 |
| Std | 484 | 653 | 338 | 468 | 32 | 87 | 387 | N/A | 135 | 239 | 102 | 526 |

J Neural Eng. Author manuscript; available in PMC 2016 May 17.

**Table 2**

Summary of all failure modes and array durations.

| Failure mode | No. of arrays | Details of failure | Time to failure | (% viable channels) | |
|---|---|---|---|---|---|
| *Acute* | | | | | |
| Mechanical | | | | | |
| Traumatic | 1 | Connector pins damaged during a seizure | | 565 (45%) | |
| | 1 | Connector pins damaged by technician | | 420 (26%) | |
| | 1 | Connector pins damaged by monkey | | 24 (N/A) | |
| | 1 | Connector removed and wire snapped by another monkey | | 201 (90%) | |
| | 1 | Connector dislodged from acrylic and snapped wire | | 496 (26%) | |
| | 1 | Array pulled from brain by monkey picking at wound | | 187 (79%) | |
| | 1 | Wire bundle severed by monkey picking at wound | | 376 (41%) | |
| | 2 | Array iatrogenically pulled from brain during surgery | 0 (N/A) | | 167 (26%) |
| | 3 | Wire bundle damaged by cortex screws and acrylic cap | 48 (6%) | 48 (42%) | 48 (46%) |
| | 8 | Connector removed and wire snapped by monkey | 748 (5%) | 43 (52%) | 30 (N/A) |
| | | | 674 (19%) | 19 (35%) | 819 (32%) |
| | | | 141 (24%) | | 27 (52%) |
| Surgical | 3 | Surgical internalization to treat epidural abscess | 62 (N/A) | 62 (N/A) | 1832 (27%) |
| | 3 | Surgical removal secondary to loose connector | 38 (67%) | 420 (21%) | 735 (21%) |
| | 4 | Surgical removal secondary to erosion of hydroxyapatite | 63 (63%) | | 119 (65%) |
| | | | 63 (48%) | | 176 (21%) |
| Biological | 2 | Death from intraparenchymal hematoma | 3 (N/A) | | 3 (N/A) |
| | 4 | Euthanasia for subdural empyema | 74 (36%) | | 30 (14%) |
| | | | 74 (36%) | | 30 (14%) |
| Material | 1 | Connector rotated within pedestal and cut wire bundle | | 84 (11%) | |
| | 2 | Defective array | 0 (N/A) | | 0 (N/A) |
| | 3 | Connector ‘short’ | 50 (14%) | 205 (6%) | 341 (24%) |
| Unknown | 3 | Acute unknown | 198 (22%) | 54 (N/A) | 0 (N/A) |
| Chronic | | | | | |
| Biological | 1 | Meningeal encapsulation following meningitis | | 261 (39%) | |
| | 3 | Meningeal encapsulation of standard arrays | 99 (6%) | 76 (5%) | 125 (33%) |